

**BUKU PROFIL PENYELIDIKAN SKIM GERAN PENYELIDIKAN
GERAN UNIVERSITI JANGKA PENDEK / GERAN DALAM UMP**

**FUNDAMENTAL STUDY OF HYBRID GRAPHENE OXIDE AND NANOFIBRILLATED
CELLULOSE FOR AIRCRAFT WINGS APPLICATION**

Assoc.Prof.Ir.Ts.Dr.Kumaran Kadirgama

MD. MUSTAFIZUR RAHMAN
WAN AZMI BIN WAN HAMZAH
DEVARAJAN A/L RAMASAMY
MAHENDRAN A/L SAMYKANO
Jose Rajan

Universiti Malaysia Pahang
kumaran@ump.edu.my
Nanofluid

ABSTRACT (120 words)

Strong synthetic fibers such as carbon fibers have an important role in a range of applications from aircraft to wind turbine blades. However, these fibers are expensive and demonstrate limited performance. The main objective is to develop well-aligned, strong microfibers prepared by hybridizing two-dimensional (2D) graphene oxide (GO) nanosheets and one-dimensional (1D) nanofibrillated cellulose (NFC) fibers and investigate the thermal physical properties. This hybrid material will have the potential to supersede carbon fibers due to their low cost and provide properties such as strength, elastic modulus and fatigue as carbon fibers. The heat carrier capability of hybrid 1D NFC and 2D GO with ethylene glycol and water mixture will be identified. Nanofluid will be prepared as two step method for thermophysical measurement. Thermal conductivity is measured by transient hot wire method using KD2-pro equipment and dynamic

viscosity is measured using Brookfield DV-III. Both the experimental results and molecular dynamics simulations can reveal the synergistic effect between GO and NFC: the bonding between neighboring GO nanosheets is enhanced by NFC because the introduction of NFC provides the extra bonding options available between the nanosheets. Molecular dynamic simulation performs to study the bonding interaction and behaviour between particles and nanofibrillate. It is expected the hybrid material can perform as carbon fiber in term of mechanical properties. The significant output will be hybrid 1D NFC and 2D GO which can be able to enhance mechanical property for high strength application and enhance thermophysical property for heat transport application. Template-assisted electrochemical deposition approach successfully synthesized high purity graphene (97.97% based on EDX analysis), 2. Qualitative analysis from FESEM images showed that all the surface texture of graphene found to be rough and flaky with rough surface texture when the deposition temperature increase. 3. XRD analysis suggests that all the grown graphene is polycrystalline in nature and the obtained XRD spectrum does not show any change in the crystal orientation when different synthesis condition was applied. However, increase in crystal size was noticed when deposition temperature increased, and it is also noted that the average of crystal size increase in small amount when the stabilizer concentration reduced. From MD simulation, the estimated elastic modulus for graphene is between 140.02 to 142.5 GPa, the yielding stress between 16.465 to 16.732 GPa and the yielding strain between 0.1181 to 0.1209. Due to the increasing demand in industrial application, nanofluids have attracted the considerable attention of researchers in recent decades. The addition of nanocellulose (CNC) with water (W) and ethylene glycol (EG) to a coolant for a radiator application exhibits beneficial properties to improve the efficiency of the radiator. The focus of the present work was to investigate the performance of mono or hybrid metal oxide such as Al₂O₃ and TiO₂ with or without plant base-extracted CNC with varying concentrations as a better heat transfer nanofluid in comparison to distilled water as a radiator coolant. The CNC is dispersed in the base fluid of EG and W with a 60:40 ratio. The highest absorption peak was noticed at 0.9% volume concentration of TiO₂, Al₂O₃, CNC, Al₂O₃/TiO₂, and Al₂O₃/CNC nanofluids which indicates a better stability of the nanofluids' suspension. Better thermal conductivity improvement was observed for the Al₂O₃ nanofluids in all mono nanofluids followed by the CNC and TiO₂ nanofluids, respectively. The thermal conductivity of the Al₂O₃/CNC hybrid nanofluids with 0.9% volume concentration was found to be superior than that of the Al₂O₃/TiO₂ hybrid nanofluids. Al₂O₃/CNC hybrid nanofluid dominates over other mono and hybrid nanofluids in terms of viscosity at all volume concentrations. CNC nanofluids (all volume concentrations) exhibited the highest specific heat capacity than other mono nanofluids. Additionally, in both hybrid nanofluids, Al₂O₃/CNC showed the lowest specific heat capacity. The optimized volume concentration from the statistical analytical tool was found to be 0.5%. The experimental results show that the heat transfer coefficient, convective heat transfer, Reynolds number and the Nusselt number have a proportional relationship with the volumetric flow rate. Hybrid nanofluids exhibit better thermal conductivity than mono nanofluids. For instance, a better thermal conductivity improvement was shown by the mono Al₂O₃ nanofluids than the CNC and TiO₂ nanofluids. On the other hand, superior thermal conductivity was observed for the Al₂O₃/CNC hybrid nanofluids compared to the other mono and hybrid ones (Al₂O₃/TiO₂).

1. INTRODUCTION

Lately, with the vast advancement in the area of nanoscience and nanoengineering, nanomaterials have received substantial attention among the researchers worldwide. The unique properties of the nanomaterials (chemical, mechanical, electrical, electronic physical) compared to the bulk materials are the driving force for the interest. The properties and the functionalities tend to significantly differ from bulk when the dimensions of the material reduced down to the nano-sized region. One-dimensional (1D) nanostructures are the structure in which they are

constrained in two directions. Within this category the 1D nanostructure materials differentiated between nanowires (aspect ratios greater than 10), nanorods (aspect ratios less than 10), and nanotubes (hollow interior). The versatile electrical, conductivity, optical transparency and chemical inertness properties are the keys to the development of novel devices such as molecular electronics, supercapacitors, touch sensors, and transparent electronics. Nanomaterials are also attractive since they can be readily fabricated or synthesized using various methods and techniques. However, the fabrication and synthesizing techniques to produce nanomaterials need to be well understood, since the processing parameters determine the quality of the produced structures. In the past two decades, researchers have studied numerous methods to synthesize the 1D nanostructure with different shapes, morphology, size, and material which has an exciting and fundamentally different configuration (Gambhire et al., 2008; J. Weber, Singhal, Zekri, & Kumar, 2008). Therefore, numbers of methods and techniques have been reported in synthesis the nanostructures with a variety of strategies, such as directly 2 catalyzed growth, template-based synthesis, and self-assembly nanowires (Guha, Chakrabarti, & Chaudhuri, 2004; Y. Y. Guo et al., 2010). Among the different methods cited in the literature, template-based synthesis is one of the well-known strategies to produce 1D nanostructures. This approach is relatively straightforward as the template serves as a scaffold within or around which a material is generated and shaped into a 1D nanostructure with the morphology complementary to the template used (Younan Xia et al., 2003). This method has been known for its simplicity, high-throughput and costeffectiveness which allow the duplication of the complex topology present on the template surface in a single step (Ghahremaninezhad & Dolati, 2009; Y. Xia et al., 2003). This method typically operates at ambient temperature, and pressure as well as can also be used for mass production of nanostructures with controlled geometry and morphology (Al-Salman, Sommer, Brezesinski, & Janek, 2015; Irshad, Ahmad, Mohamed, & Abdullah, 2014; Şişman, 2011; Zheng, Zhang, Li, & Shen, 2002). A number of different synthesis techniques used in conjunction with templates have been tried by various researchers around the world. However, the most prominent and efficient routes are the electrochemical deposition (Brumlik, Menon, & Martin, 1994; Mohanty, 2011), sol-gel (Z. Y. Wang et al., 2011), chemical vapor deposition (X. D. Li et al., 2011) and pressure injection method (Phillips, Fang, Zheng, & Lagoudas, 2011). The synthesis methods together with the different type of templates have been shown to generate 1D nanostructures like nanorods, nanotubes, and nanowires composing from various type of materials

The channel tank comprises tubes and blades that placed in the center and allows the stream of coolant to pass through and ingest the heat. The hot coolant, which retained the heat, will then be guided from the tubes to balances. The cool air from outside is then pickups up the heat leaving the cooled coolant for next cycle (Amrutkar and Patil 2013).As mentioned above, there are several different types of radiator coolants are available in market, however, only a few of them can give proficient constrained convection heat exchange between the radiator and the

engine. An ideal radiator coolant for car engine should have superior heat retention properties since the car engine needs to work productively through elevations, climate, and extraordinary road conditions. As such, the aims of the present work is to develop and enhance the performance of a radiator coolant comprising of Ethylene Glycol (EG) and Nanocellulose (CNC) from Canadian hemlock plant, Titanium dioxide (TiO_2) and Aluminium oxide (Al_2O_3) may improve the heat transfer behaviour and eventually overcomes the overheating issue experienced by the car engine. Heat transfer has been an important criterion for many industrial types of equipment and machinery. Most of this industrial facility and machinery requires proper heat transfer management from different phases for efficient productivity (Sivashanmugam 2012). Thus, an efficient heat transfer fluid is required for best heat management and efficient process. Correspondingly, the swift increase in energy demand further necessitates the need for enhancement in the heat transfer process and reduction in energy loss due to the inept use of the system. Specifically, in an automotive application, coolants and oils are used as a heat transfer medium. As the name implied, coolant plays a significant role in reducing the heat in the automotive components. However, common base fluids such as water, and ethylene glycol reported having inadequate heat transfer properties, thus decreasing the performance of automobile components and its efficiency. As such, it has paved to the development of a new fluid called nanofluids which expected to have that high thermal performance. Angayarkanni and Philip (2015) stated that there are three traits required for nanofluids to be an effective coolant. Which are enhanced thermal conductivity, better heat transfer, and improved critical heat flux. In nanofluids, the heat properties are usually improved by introducing high thermophysical properties nanoparticles into the heat transfer fluids. At present, one or two different type of nanoparticles commonly metal oxide are dispersed in the common base fluid like water and ethylene glycol and their behavior are studied.

2. RESEARCH METHODOLOGY

First of all, it is essential to define the system that is going to be simulated in MD simulation. The established dimensions of the modeled nanowires and also the initial position of the atoms need to be defined at the first step of MD simulation. Once these elements are identified, and a potential function is selected a time step has to be chosen. The simulations begin by defining the forces between atoms for the specific system. Through the use of time integration to resolve the equations of motion, the atoms of the structure in the simulation are forced to be moved to a new position. Once this new state or position has been reached, the time is advanced (one time step) to continue with the simulation. These steps are continuously repeated until the simulation comes to about conditions imposed previously or until it reaches a specified number of time steps. The procedure below show the steps on how the MD simulation runs:

- The initial velocity and position of every atom are defined.
- The forces between atoms are calculated using the interatomic potentials.
- Once the forces are obtained, the small time intervals, the initial atomic positions, and velocities changed to a second state following classical dynamics equations of motion.
- When the new locations and velocities are known, the forces re-calculated and the procedure repeated until the end of the simulation.

The primary assumptions in this simulation are; no mass

changes in the system during the simulation. During the simulation, it is expected no additional atoms enter or leaves the simulation box. Therefore, the total energy of the system must remain constant until the simulation end. Limitation of the MD simulation The simulations performed must be in the range of validity, to draw out the valid conclusions from the simulation, It is a powerful technique but also has some limitations that have to be taken into account Interaction between atoms While simulating a bulk of atoms, the realism of forces which describe the interaction between atoms must be considered. Atoms move when there is the action of instantaneous forces resulting in the changes of their initial position, and the forces change as well. The representation of the interatomic forces influences the accuracy of the simulation results. Since the forces are obtained from the gradient of a potential energy function, the practicality will depend on the ability of the chosen potential to reproduce the behavior of Ni nanowires. Time and size limitations MD simulations are capable of simulating systems with thousands of atoms, and at the same time with large space-time resolution. With MD it is feasible to focus on a system with time ranging from hundreds of nanoseconds (nsec) to only a few picoseconds (psec). Despite to this possibilities, it also may have some limitations due to the capability and efficiency of the computer. Boundary Condition Considering that the simulated system will be tiny compared to the macro size materials, the fraction of the number of surface atoms and the total number of atoms will be different from the actual. These defines that most of the atoms will be found on the surface of the domain and have fewer neighbors. As a result, the surface effects will be more prominent, which also the reason for periodic boundary conditions often used for nanoscale simulations. The periodic boundary conditions consist the replication of a simulation box where the molecules are walled. Simulation Time Step In MD simulations, the time step is an essential parameter as it will determine the total simulation time and also the computational power (expense) required. Three main criteria need to be followed to choose right time step are; (1) the time step should be small enough so that the simulation is realistic, (2) time step should be sufficient but that the simulation, not very long and (3) the atoms motion is continuous

The fluid was prepared by mixing water and EG with a certain percentage. The volume of prepared mixture was equal to the total volume of the radiator during standard procedure in an automotive engine. For example, if the volume of the radiator is 1 L, then the volume of individual cooling fluid in the radiator. In the present study, the radiator with the volume of 4 L was used for observation. Accordingly, 3.9 L of nanofluid is prepared for 0.5% volume concentration. The volume of nanocellulose and aluminium oxide were determined by using equations 3.1 and 3.2 as shown below.

$$\phi = \frac{\omega \rho_w}{\left(1 - \frac{\omega}{100}\right) \rho_p + \frac{\omega}{100} \rho_w} \quad (\text{Eqn. 1})$$

$$\Delta V = (V_2 - V_1) = V_1 \left(\frac{\phi_1}{\phi_2} - 1\right) \quad (\text{Eqn. 2})$$

Before the synthesis, all the glassware such as beaker, measuring cylinder and syringe were cleaned properly. In a typical procedure, firstly, 368 mL of distilled water was taken in 1L beaker followed by 552 mL of EG. The ratio of water to EG was 40:60. Further, 70 mL nanocellulose was dispersed in above base fluid of distilled water and EG using a syringe. The mixture was magnetically stirrer for 30 min to ensure the homogeneous dispersion of nanocellulose in water and EG solution. Finally, the mixture was sonicated for 2 h at 50 °C temperature.

Characterization Techniques

X-Ray Diffractometer (XRD)

X-ray powder diffraction (XRD) is a rapid critical technique and primarily used for examining intricate phase classification of a crystalline material including atomic arrangement and crystallite size. In 1912, Max von Laue, exposed that crystalline substances work as three-dimensional diffraction gratings for X-ray wavelengths similar to the spacing of planes in a crystal lattice. X-ray diffraction is based on constructive interference of monochromatic X-rays. These X-rays generated from cathode ray tube, are filtered to produce monochromatic radiation, collimated to concentrate, and directed toward the target. According to Bragg's Law, the interaction of the incident rays with the sample produces constructive interference (and a diffracted ray). For example, the characteristic Cu K α X-rays with a given λ are incident at angle θ on the planes of the crystal or polycrystalline powder comprising lattice planes with a spacing d , these rays will be 'reflected' from the planes as shown in Figure 3.1. The path difference (MQ+QN) between the X-rays reflected from successive planes will be $2d \sin\theta$. According to Bragg's law, the reflected rays will have constructive interference when the path difference is an integral multiple (n) of λ :

$$n\lambda = 2d \sin\theta \quad (\text{Eqn. 3.})$$

These diffracted X-rays are then detected by the detector and counted by the counter. By measuring the intensity of scattered waves, a diffraction pattern is observed as a function of scattering angle. Sample is scanned through a range of 2θ angles, all possible direction of diffraction of the lattice should be attained owing to the random orientation of the powdered material. Conversion of the diffraction peaks to d -spacing provides the identity of the mineral because each mineral has a set of unique d -spacing. Typically, this is achieved by comparison of d -spacing with standard reference patterns.

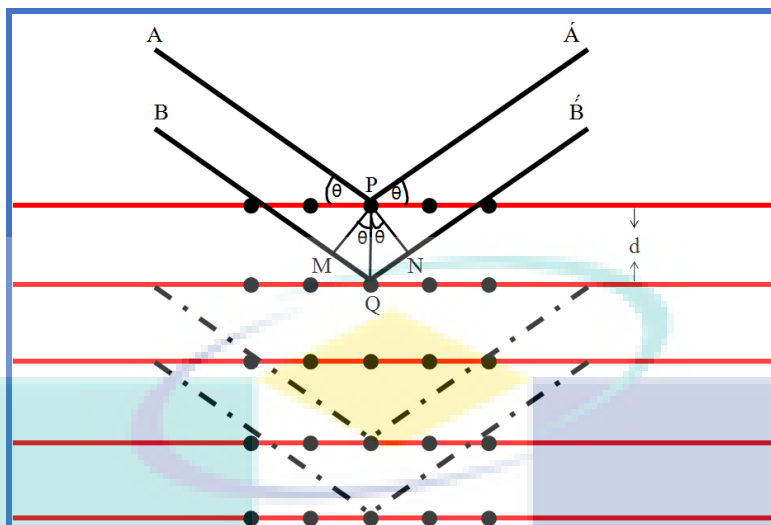


Figure 1 Schematic representation of X-ray diffraction

Fourier Transform Infrared (FTIR) Spectroscopy

FTIR is one of the most versatile and important analytical technique for the measurement of functional groups in organic as well as inorganic samples. It provides qualitative information about the compound in mixture. Infrared spectroscopy is mainly based on the vibration of molecules. The working principle of FTIR spectroscopy is represented in Figure 2.

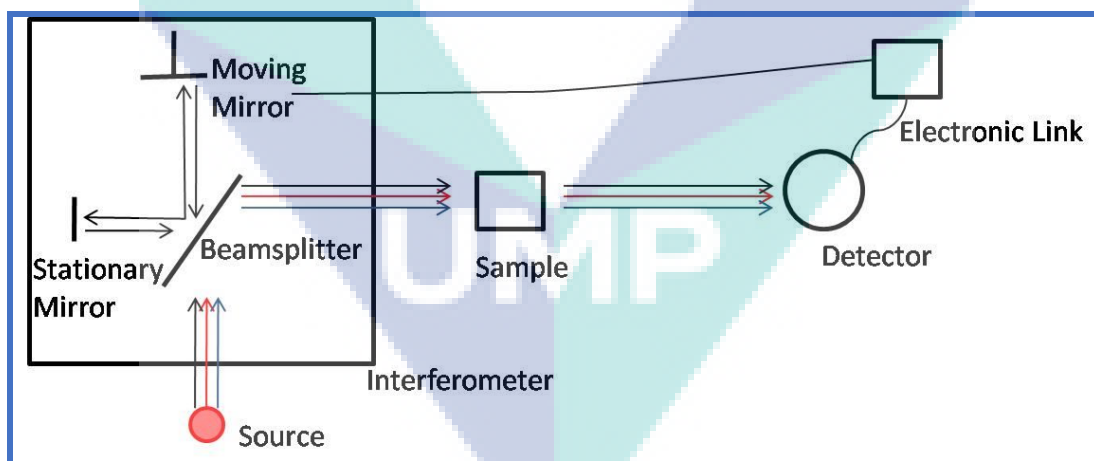


Figure 2 Schematic representation of FTIR spectroscopy

When an IR radiation passes through a specimen, some radiation is absorbed at a particular energy which provides IR spectrum. The absorption peak observed at a particular energy is due to vibration of a particular band. In the present work, the Fourier transform infrared (FTIR) spectrum was recorded with spectrometer using KBr (Potassium bromide) pellet method. Typically, sample (1 to 2 mg) was mixed well with KBr (200 mg) using mortar pestle and then

pressed into pellets using hydraulic press (pressure ~150 psi for 30 sec). Then, these transparent pellets were scanned over the range of 2000 cm^{-1} -400 cm^{-1} .

Field Emission Scanning Electron Microscopy (FESEM)

FESEM is a nondestructive technique. A beam of electron is employed to the specimen to generate variety of signals in FESEM. FESEM is mainly used to study the topography, chemical composition, and orientation of materials. In FESEM, electron beam of a sufficient kinetic energy interacts with the specimen and generate signals including secondary electrons (SE), backscattered electrons (BSE), photon etc. Generally, secondary and backscattered electrons are used for imaging. X-rays (in Energy dispersive analysis of X-rays-EDAX) generated during interaction gives information about elements present in the specimen. Usually tungsten filament is used as electron source (gun), whereas for higher resolution, field emission gun (FEG) is required. The electrons are generally accelerated from 1keV to 30 keV. In the present work, field emission scanning electron microscope is used for analysis. EDAX utilizes X-rays emitted from the surface during FESEM measurement. This method involves the qualitative as well as quantitative measurement of element present in the specimen. When an accelerated electron beam hits any specimen, it emits X-rays which is specific for each element. The minute amount of specimen is poured on carbon tape placed on a tab and then gold coated for 90 sec.

Transmission Electron Microscopy (TEM)

Transmission electron microscope (TEM) utilizes transmitted electrons through the specimen and gives information about crystal structures, defects, chemical analysis, growth mechanism and grain boundaries. Further the magnification that can be attained in TEM is higher than that of SEM as high energy electrons ($> 50 \text{ keV}$) are used in TEM. The working principle of TEM is similar to SEM, only the interaction between transmitted electrons and specimen provides images. In TEM analysis more information can be extracted from diffracted electrons. To obtain high quality image in TEM analysis, sample preparation is very important. Sample was dispersed in distilled water using ultrasonicator for 15 min. Then, the suspension was poured on carbon coated copper grid (200 meshes) and air dried. This grid is used for analysis.

Thermophysical Properties

The thermal properties of nanofluids depend upon various process and system parameters such as preparation method and surface chemistry of nanoparticles etc. Further, stability of nanofluids which is a very important factor, also depends on the preparation method. For example, a nanofluid with homogenous dispersion of nanoparticle shows better performance

than the inhomogeneous nanofluids. An inhomogeneous dispersion of nanoparticle may result of sedimentation, agglomeration and erosion on metal surfaces (Lee and Mudawar 2007).

(i) Density (ρ_{nf}):

Density is a measure of how heavy an object is for a given size, i.e. the mass of material per unit volume. It does not depend on amount or shape of the material, but varies with temperature and pressure. The S.I. unit of density is grams/milliliter (g/mL) or grams/cubic centimeters (g/cm³). Firstly, the base nanofluids have been identified by measuring the densities and comparing with standard (ASHRAE 2005). In addition, the types of nanofluid will be estimated by measuring the densities.

The density (ρ_{nf}) of nanofluid has been calculated by using the Equation 3.4: [(Choi and Eastman 1995); Wang et al., 1999; (Das, Putra et al. 2003), Wen and Ding, 2004; Heris et al., 2007; Trisaksri and Wongwises, 2007; Zhou and Ni, 2008; Williams et al., 2008; Das et al., 2008; Duangthongsuk and Wongwises, 2010, Demir et al, 2011, Sharma et al, 2012; Fedele et al., 2012; Kayhania et al, 2012]:

$$\rho_{nf} = \phi\rho_p + (1 - \phi)\rho_f \quad (\text{Eqn. 4})$$

The performance of base fluid (water, EG, 10% EG-90water and 20% EG-80% water) has also been compared with standard (ASHRAE, 2005).

(ii) Specific Heat Capacity (C_{nf})

Specific heat capacity (C_{nf}) can be defined as total amount of heat required to increase the temperature of a matter by one per unit mass. C_{nf} of nanofluid was estimated by using Equation 3.5: [Lee; 1999; Duangthongsuk and Wongwises, 2009; Putra, 2003; Trisaksri, 2007; Choi, 1999; Wen, 2004; Williams, 2008; Heris, 2007; Zhou, 2008; Fedele, 2012; Sharma, 2010; Gosselin, 2004; Ho, 2010].

$$C_{nf} = \phi C_p + (1 - \phi)C_f \quad (\text{Eqn. 5})$$

where C_{nf} , C_f , and C_p are the specific heat of nanofluid, base fluid and nanoparticles, respectively. The device, shown in Figure 3.1, was used to measure the specific heat capacity of nanofluid in (J/kg. °C). Initially, the device was calibrated by measuring the specific heat capacity of standard fluid (Glycerin) and then measurements were carried out on nanofluid and base fluid.

(iii) Thermal Conductivity

The transient hot-wires process has been used to measure thermal conductivity of nanofluids (shown in Figure 3.3). Platinum has high electrical resistivity i.e. $1.06 \times 10^{-7} \Omega \text{ m}$ (at $20 \text{ }^\circ\text{C}$) and temperature coefficient resistance of $0.0003925 \text{ }^\circ\text{C}^{-1}$ and both are of greater magnitude than other metals as the material of the wire. The wire is to be used as a line heat source, so the wire diameter is usually kept within $100 \mu\text{m}$. The length of the wire is kept to just a few centimeters, which compared to the wire diameter represents an infinitely long line heat source, assuring one directional (radial) heat transfer. Calibration process has also been done with standard fluid (Glycerin) before measurement.

A number of studies have been reported in the literature on experimental and theoretical studies of thermal conductivity model of nanofluid. In the present work, three models have been adopted to determine the thermal conductivity of nanofluid. The Maxwell model is the first model that has been proposed for solid-liquid mixture with relatively large particles. It is based on the solution of heat conduction equation through a stationary random suspension of spheres (Maxwell, 1891) as per Equation 3.6a and 3.6b:

$$\frac{k_{nf}}{k_f} = \frac{k_p + 2k_f + 2\phi(k_p - k_f)}{k_p + 2k_f - \phi(k_p - k_f)} \quad (\text{Eqn. 6a})$$

Bruggeman was proposed a model to study the interactions between randomly distributed spherical particles (Bruggeman, 1935) as:

$$\frac{k_{nf}}{k_f} = \left[(3\phi - 1) \frac{k_p}{k_f} + (3(1 - \phi) - 1) \right]^2 + 8 \frac{k_p}{k_f} \quad (\text{Eqn. 6b})$$

For non-spherical particles, Hamilton and Crosser developed a model for effective thermal conductivity of two component mixtures. The model is based on the thermal conductivity of both the base fluid and the particle, volume fraction and shape of the particles (Hamilton and Crosser, 1962) as per Equation 3.6c:

$$\frac{k_{nf}}{k_f} = \frac{k_p + (n-1)k_f + (n-1)\phi(k_p - k_f)}{k_p + (n-1)k_f - \phi(k_p - k_f)} \quad (\text{Eqn.6c})$$

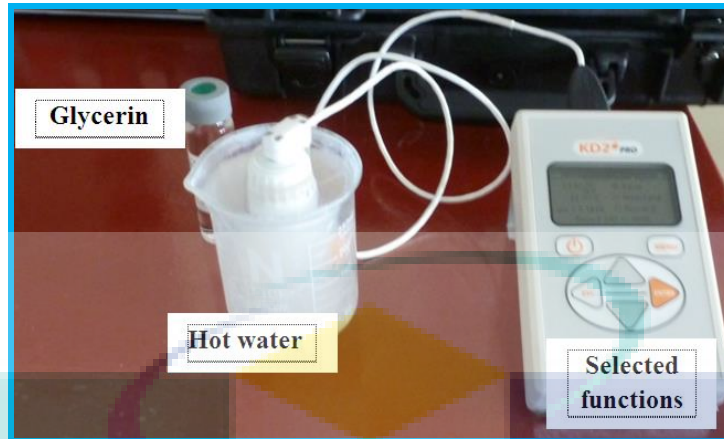


Figure 5 Thermal conductivity and heat capacity device

(iv) Viscosity

Viscosity is another important factor to evaluate the thermal properties of nanofluids. Commercial Brookfield DV-I prime viscometer (shown in Figure 3.4) was used to measure viscosity of nanofluids at different temperatures and rotor (rpm).

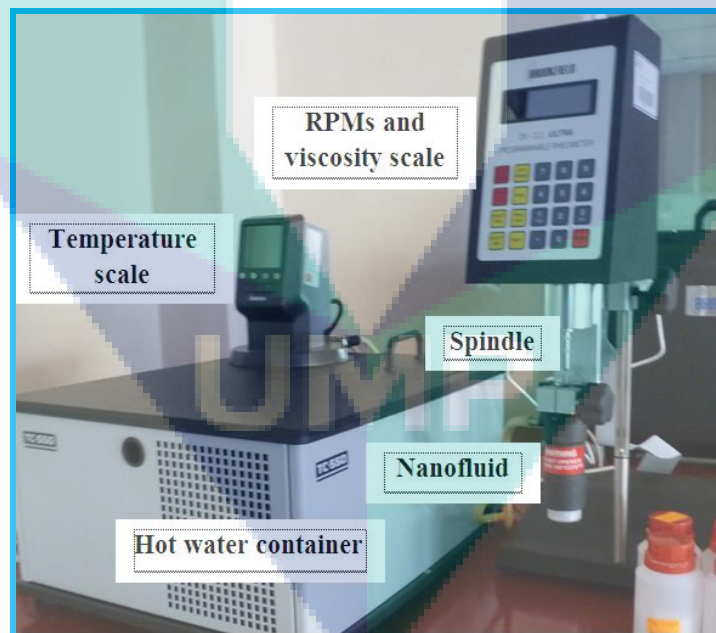


Figure 6 Brookfield DV-I prime viscometer

This type of viscometer are generally used for Newtonian and non-Newtonian liquids having from low to high viscosity values (depending on the spindle, from 1 to 600 cP).

Viscosity of nanofluid (μ_{nf}) has also been estimated theoretically. A numbers of viscosity models have been reported to find the effective nanofluid viscosity as a function of volume concentration (shown in figure 3.5).

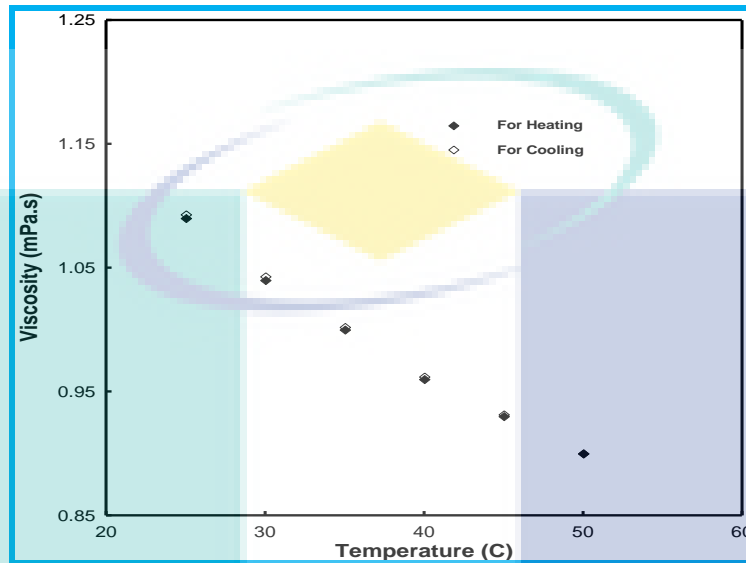


Figure 7 Viscosity calibration for pure water

Einstein (1906) determined the effective viscosity of a suspension of spherical solids as a function of volume concentration lower than 5% using the phenomenological hydrodynamic Equation 3.7a:

$$\mu_{nf} = (1 + 2.5\phi)\mu_f \quad (\text{Eqn. 7a})$$

Several equations have been developed in an effort to extend Einstein's formula to suspensions of higher concentrations, including the influence of non-spherical particle concentrations like Brinkman (Brinkman 1952) as in equation 3.7b:

$$\mu_{nf} = \frac{1}{(1-\phi)^{2.5}} \quad (\text{Eqn. 7b})$$

The effect of Brownian motion on the effective viscosity in a suspension of rigid spherical particles was studied by (Batchelor 1977) and propose an mathematical formula which can be expressed as Equation 3.7c:

$$\mu_{nf} = (1 + 2.5\phi + 6.2\phi^2)\mu_f \quad (\text{Eqn. 7c})$$

Lundgren proposed the following equation under the form of a Taylor series (Lundgren 1972) as Equation 3.7d:

$$\mu_{nf} = \frac{1}{1-2.5\phi} \mu_f \quad (\text{Eqn. 7d})$$

Test Rig Setup

The schematic diagram of the used radiator test rig is shown in Figure 3.6. A 24 V DC supply was used as main power source for pump and heater. The radiator test rig is a closed loop system where water circulate in the system by water pump.

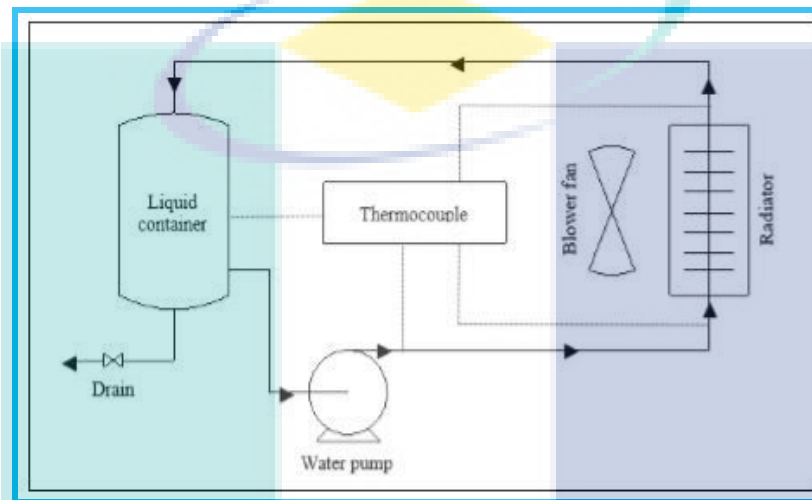


Figure 8 Schematic diagram of radiator test rig

There are K-Type thermocouples at four points on radiator wall to measure the surface temperature of the radiator. A 12 V cooling fan is attached to the radiator which act as normal radiator fan similar to readily available automobile radiator. Heat produced from an automobile system during its routine is imitated by a 1kW heater. 4 L of the essential coolant fluids composed of nanofluid and distilled water is stored in a 5 L metal tank.

3. LITERATURE REVIEW

Sainath et al., (G. Sainath, Choudhary, & Jayakumar, 2015) state that the complexities involved in performing experiments at small length scales prevent the evaluation of mechanical properties using conventional testing methods. In contrary, the simulation with suitable inter-atomic potentials can provide appropriate deformation and damage mechanism operative at the nanoscale. Mustafa and Sakir (Kurban & Erkoç, 2016) stated that the MD simulation results give the structural information as well as thermodynamic value, which help the chemist further with synthesis and development of new functional nanostructured materials. MD is a computer simulation that dynamically analyzes physical movements of atoms and molecules behavior and provides a means of evaluating predictive properties invoking principles of statistical mechanics.

It shows a different approach to evaluate the material properties that focused on the atomic scale, which is the smallest entities of materials. To date, most of the research on the deformation behavior of metallic nanowires has been carried out by computer simulation, especially using MD method. Gall et al., (Gall, Diao, & Dunn, 2004) studied the mechanical properties of gold nanowires by using MD simulation and provided the fundamental understanding of the gold nanowire strength. MD simulations are based on the following underlying principles. First, all the molecules and atoms are described as a system of interacting material points. The procedure in using MD consist of few steps: The initial position and velocity of every atom are described. • The forces between these atoms are calculated by using the interatomic potentials. • Once the forces are known, a small time intervals, the initial atomic positions and velocities changed to a second state following classical dynamics equations of motion. • When the new positions and velocities are known, the forces are re-calculated, and the procedure is repeated until the end of the simulation.

Latterly, nanocellulose research has received significant attention as it has shown for a potential application in biomechanics, foods, electronics, and automotive fields. Nanocellulose is a nature-based nanomaterial (natural material) that has superior material behavior, especially at the nanoscale to be used in various applications.

Nanocellulose has also been reported to have a great advantage in terms of sustainability, abundance, mechanical properties such as large surface to volume ratio, high tensile strength and stiffness, high flexibility, and good electrical and thermal properties. Moreover, nanocellulose is also a safe and environmentally friendly material to handle and consume.

Automotive industries are among the huge engineering sector which deals with heat transfer properties studies. Apart from the best design, safety and aesthetic values, efficiency and low fuel consumption is another important aspect. The cooling system contributes significantly to the efficiency and eventually the fuel consumption of a car (Bhatt, Patel et al. 2014). Therefore, to improve the efficiency of an automobile system, it is important that the fundamental studies related to the heat transfer mechanism are undertaken.

The state-of-the-art development in nanotechnology has led to the invention of novel fluid so-called nanofluid which contains nanoparticles with an average size of 100nm. This fluid has been shown and reported to have improved heat transfer properties which could improve the efficiency of a cooling system.

Studies have shown that these nanofluids have better thermal physical properties compared to conventional cooling fluids for enhanced heat transfer performance. Their thermal behaviour has also been reported to surpass the cooling liquids encasing particles of micrometer

size (Peyghambarzadeh, Hashemabadi et al. 2011). As such, finding clearly shows that the nanofluids will be the next generation cooling fluids for various heat transfer applications as shown in table 2.1.

Table 1 Summary of previous studies related to nanofluid

Nanoparticles	Base Fluid	Vol. Fraction of Particles	Thermal Conductivity Enhancement	Heat Transfer Enhancement
Al ₂ O ₃	Water	1%	3%	45%
Al ₂ O ₃	Water	-	15%	40%
Al ₂ O ₃	Water	4.30%	30%	-
Al ₂ O ₃	Engine Coolant	3.5%	10.41%	-
CuO	Ethylene Glycol and Water	-	-	Improvement in convective heat transfer coefficient
Al ₂ O ₃				

Source: (Bhatt et al., 2014)

The capability of a material to behave to heat is known as thermal conductivity. It is exemplified as the rate of heat transfer through a unit thickness of the material per unit area per unit temperature difference (Cengal et al., 2013). As to date, quite a number of investigations performed with the aim to improve the heat transfer efficiency as shown in table 2.2. Among all the work that has been carried out, the liquid suspended with metals particles has been of interest. This is because the thermal conductivity of fluid that encompasses suspended solid metallic particles shown to be substantially enhanced (Choi and Eastman 1995).

Table 2: Thermal conductivity (W/m-K) of various material at 300 K

Material	Thermal Conductivity
Metallic Solids	
Aluminium	237
Non-metallic Liquids	
Water	0.613
Engine Oil	0.145

Source: Cengal et al., (2013)

The thermal conductivity properties of engineered nanofluids reported to differ with the size, shape and type of nanoparticles. For example, non-metallic (oxide) nanoparticles have lower thermal conductivity properties compared with metallic nanoparticles. Nanofluid with smaller particles size has greater thermal conductivity than the bigger ones. The shape of the nanoparticles has also been shown to influence the thermal behavior of the nanofluid. Nanofluid containing cylindrical-shaped nanoparticles exhibit greater thermal conductivity compared to the spherical shape (Murshed, Leong et al. 2008).

The amount of nanoparticles suspended in the base fluid reported to significantly influences the thermal behavior of the fluid. Usually, for research-based investigations, the quantity nanoparticles used is between 0 to 10 vol.% and subjected to a working temperature between 10°C to 50°C to validate the influence of volume concentration on viscosity, specific heat, density and thermal conductivity of the nanofluid. Previous work from several researchers has proved that the viscosity, density and thermal conductivity of the nanofluid increases proportionally with the increase in volume concentrations (Elias et al., 2014). (Dhaiban 2016) has studied the thermal properties of Zinc Dioxide-Ethylene Glycol (ZnO₂-EG) based nanofluids and reported 26.5% improvement in thermal conductivity just by adding 5% volume fraction of Zinc Dioxide nanoparticles into the base fluid ethylene glycol (Nguyen, Roy et al. 2007).

Meanwhile, an investigation on convective heat transfer measurement using Alumina-water as shown in Figure 2.12 (Al₂O₃/water) nanofluids also revealed improved heat transfer coefficient as the concentration of nanoparticles increased (Zeinali Heris, Nasr Esfahany, & Etemad, 2007). Where else, a study using nanofluids containing 170nm Silicon Carbide particles (3.7% volume concentration) showed improvement up to 50-60% in Reynolds number and heat transfer coefficients (Mintsa, Roy et al. 2009). In another study using Copper Oxide/water-based nanofluids (Figure 2.13) also revealed improvement in heat transfer coefficient when the volume concentration used is between 0-4% (Naraki, Peyghambarzadeh, Hashemabadi, & Vermahmoudi, 2013).

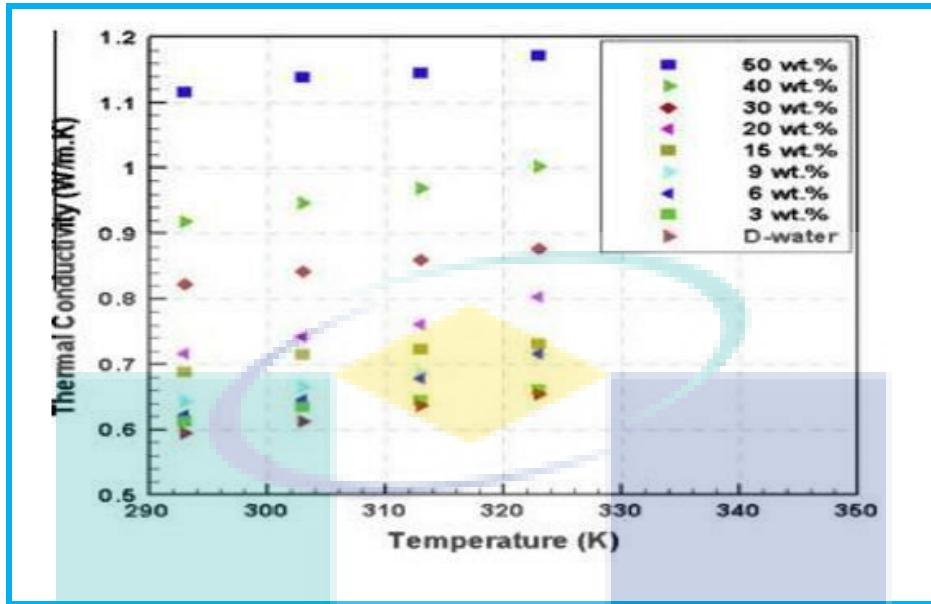


Figure 9 Thermal conductivity of Al_2O_3 -Water nanofluids at different concentration
 Source: (Ghanbarpour, Bitaraf Haghigi, & Khodabandeh, 2014)

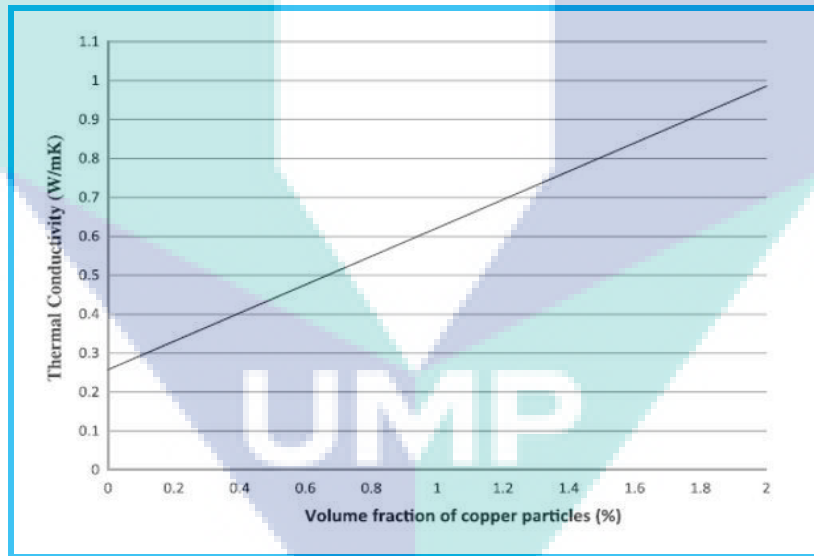


Figure 10 Thermal conductivity of EG based copper nanofluids
 Source: (Leong et al., 2010)

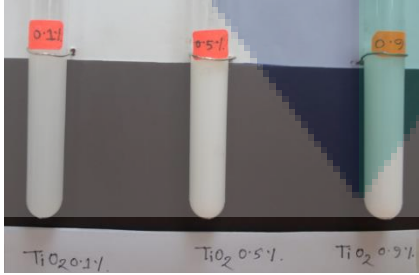
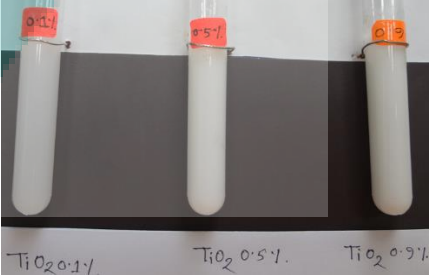
4. FINDINGS

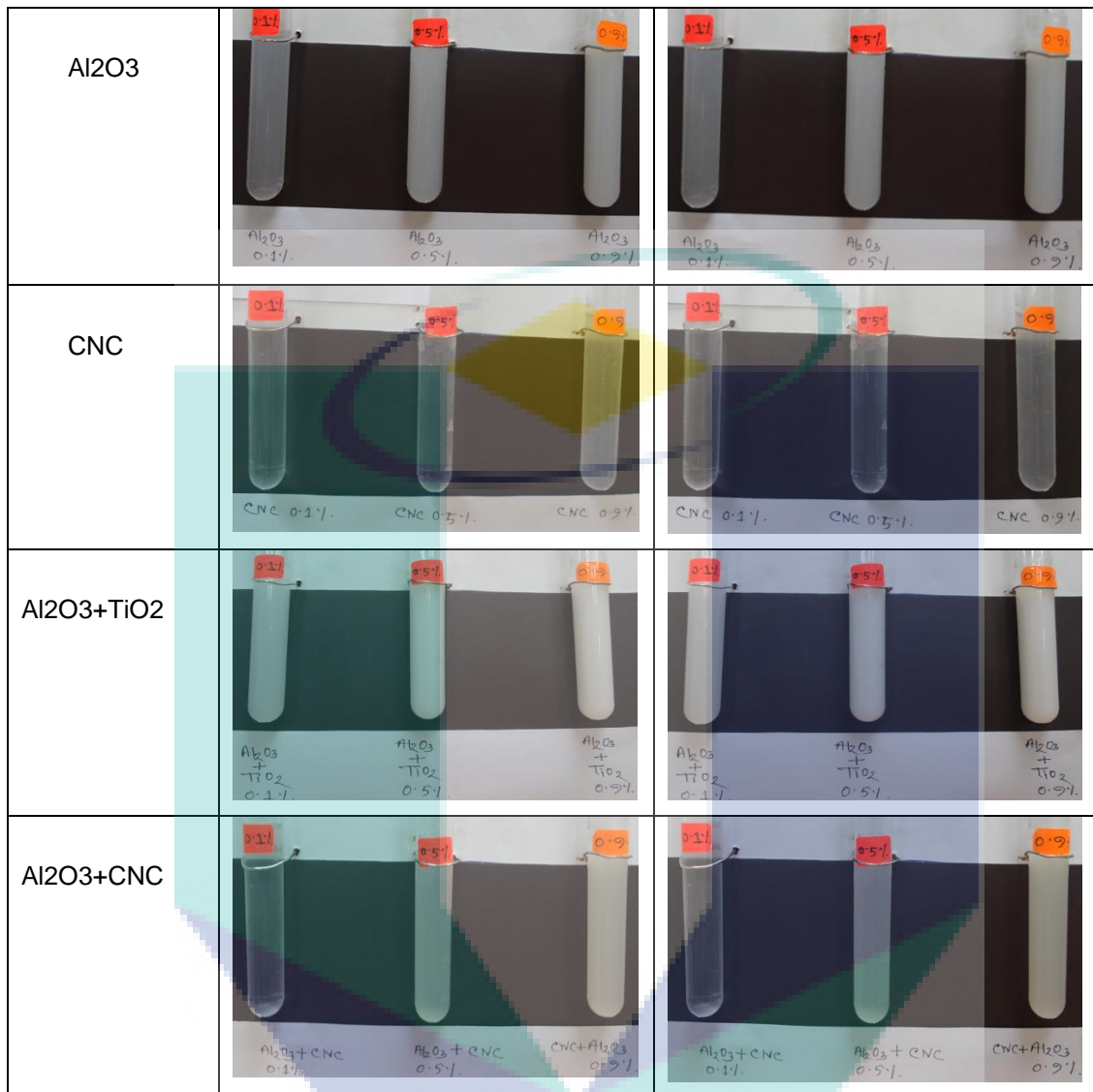
Generally, agglomeration and rapid settling of particles are some of the problems, faced by suspended particles in the fluid (Hadadian, Samiee et al. 2013). Although, heat transfer enhancement directly depends upon high durability and better stability of suspended particles in the fluid. In the present work, sonication process has been used for the preparation and control the stability of nanofluids. Esfe, Esfandeh et al. (2019) prepare more stable nanoparticles without

agglomeration by increasing the time of sonication process and observed that the test solutions containing fixed volume ratio of base fluid (EG:W) with different volume concentration test are highly stable for more than one month. The sedimentation observation of all the samples i.e., Al₂O₃, TiO₂ nanoparticle, nanocellulose CNC, hybrid (Al₂O₃ + TiO₂) nanoparticle and hybrid (Al₂O₃+CNC) nanocomposite after 6 weeks are shown in table 4.1. It was observed that the sedimentation occurs in the samples after 6 weeks. Sarafraz, Hormozi et al. (2014) reported that sedimentation in nanofluids occurs due to the strong van der Waals force.

As discussed in previous chapter, sedimentation method is generally used to investigate the stability of nanofluid. Supernatant concentration is also an important factor to control the stability of nanofluid. In the present work, Al₂O₃/CNC and CNC have been prepared without using any surfactant and found that the solutions remain stable with minimum sedimentation even after one month. The nanofluids found to be stable also during the thermos-physical investigation and the force convection experiment. Similar results were also found by (Rao, Sreeramulu et al. 2017) and reported that nanofluids remain stable up to three months by increasing the timing of ultra-sonication process. Rao, Sreeramulu et al. (2017) reported the thorough investigations on effect of sonication process for the synthesis of ZrO₂/water nanofluids. They obtained some surprising results where sonication process routed nanofluid exhibits a better thermal conductivity enhancement, suitable for cooling application. Further, observation for more than one month indicates that nanofluid displayed small amount of sedimentation in all base fluid may be due to the gravitational forces. Stability upto one month of Fe₃O₄ nanoparticles dispersed in a water-ethylene glycol mixture has also been reported by (Sundar, Singh et al. 2013). On aging, the particles aggregates may be due to high surface-activity (Narayanan and El-Sayed 2008).

Table 4 Qualitative stability evaluation of mono and hybrid nanofluids.

Nanofluids	After preparation	After 6 week
TiO ₂	 <p>TiO₂ 0.1% TiO₂ 0.5% TiO₂ 0.9%</p>	 <p>TiO₂ 0.1% TiO₂ 0.5% TiO₂ 0.9%</p>



In the present work, Transmission electron microscope has been used to acquire the high resolution image of Al₂O₃, CNC, TiO₂, TiO₂ + Al₂O₃ and Al₂O₃ + CNC in nanofluid with high magnification and results are shown in Figure 4.1 – 4,5, respectively. However, contrast and resolution was limited while acquiring the image of Al₂O₃ and CNC which may be due to low electron densities and low profile (thin). It was observed from the literature, for precise TEM imaging, well dispersed CNC sample can be successfully prepared by increasing the dispersion time with surfactant as well as by using an appropriate grid surface (Fortunati, Armentano et al. 2012, Fortunati, Peltzer et al. 2012). Among all sample preparation method, dunk method was found to be more consistent method for TEM imaging of individual CNC without using radioactive stain or an expensive glow-discharge device (Fortunati, Peltzer et al. 2012).

The TEM image of Al_2O_3 nanoparticles dispersed evenly into base fluid is displayed in Figure 4.1 which illustrates that particles are almost uniformly dispersed in base fluid with very small aggregation. Figure 4.2 shows the TEM image of dispersed TiO_2 nanoparticles into the water/ethylene glycol fluid. It is observed from the figure that TiO_2 particles have almost uniform morphology which somewhat interconnected to each other. However, particles are seems to nearly homogeneously dispersed in the base fluid. TEM micrograph of CNC nanoparticles dispersed in base fluid is represented in Figure 4.3. It can be clearly shown that the CNC nanoparticles completely homogeneously dispersed in fluid which is the one of main requirement of the present application. Figure 4.4 and 4.5 demonstrate the TEM micrographs of $\text{Al}_2\text{O}_3/\text{TiO}_2$ and $\text{Al}_2\text{O}_3/\text{CNC}$ hybrid nanofluid, respectively. It is observed that the dispersion of Al_2O_3 and TiO_2 nanoparticle are approximately uniform in the base fluid, however, both type of nanoparticles are not completely interconnected to each other. On the contrary, it can be clearly seen from the figure 4.5 that $\text{Al}_2\text{O}_3/\text{CNC}$ hybrid nanofluid are disperse uniformly in the fluid. Further, Al_2O_3 and CNC nanoparticles are completely interconnected to each other i.e., agglomerated particles which result in strong stability enhancement. Philip, Shima et al. (2008) reported that formation of agglomerated particles in the nanofluid basically depends upon on the surface contact between the particles. A strong van der Waals force works between the agglomerated particles which is very hard to break it into primary nanoparticle (Bhanvase, Sarode et al. 2014, Azmi, Hamid et al. 2016).

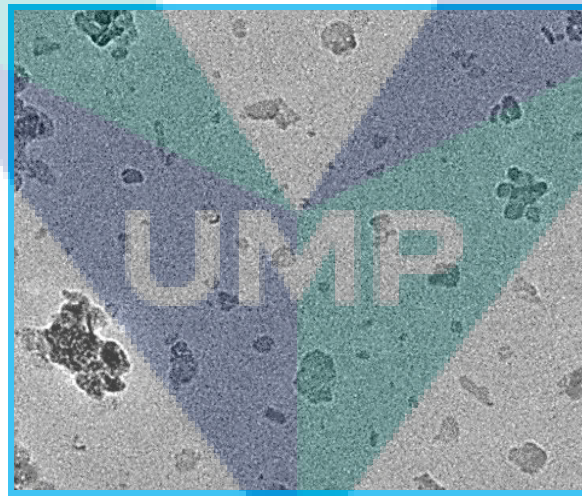


Figure 10 TEM image of Al_2O_3 dispersed nanofluids (Magnification X19,000)

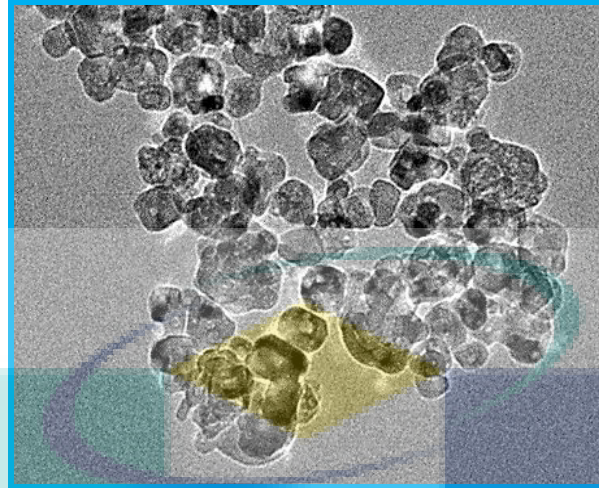


Figure 11 TEM image of TiO₂ dispersed nanofluids (Magnification X29,000)

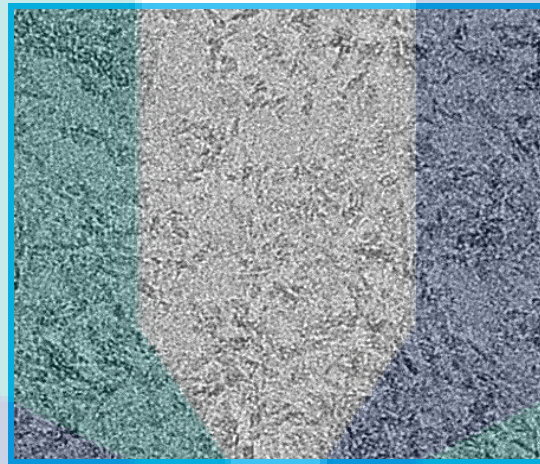


Figure 12 TEM image of CNC dispersed nanofluids (Magnification X50,000)

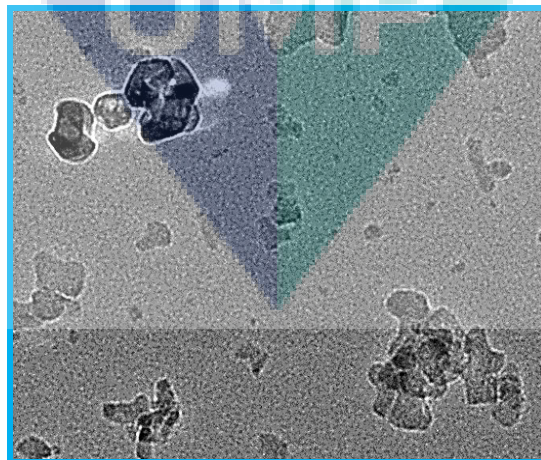


Figure 13 TEM image of Al₂O₃/TiO₂ dispersed nanofluids (Magnification X50,000)

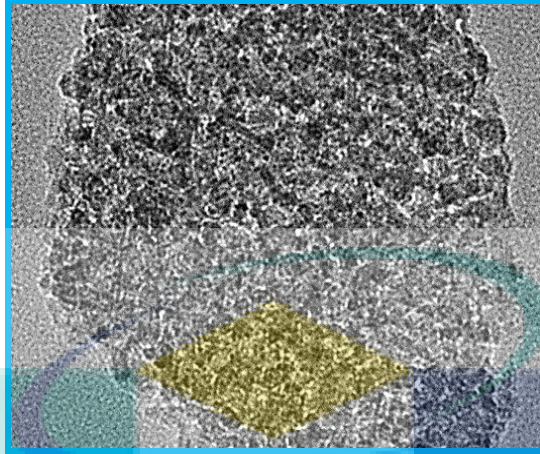


Figure 14 TEM image of Al₂O₃/CNC dispersed nanofluids (Magnification X62,000)

Estimation of absorbance drop is another measurement technique to validate the stability of nanofluid scientifically where the peak absorbance of the suspended nanoparticles at very first dilute suspension measured by scanning it. Therefore, in the present work, Ultra Violet–Visible spectrophotometer (UV–Vis) has been used to evaluate the stability of nanoparticles dispersed base fluids. The UV–Vis spectrum of all the as-prepared nanofluids with all the volume concentration were recorded in the wavelength range from 200 to 800 nm and the results are shown in Figure 4.6 – 4.10. It can be observed from all the UV-Vis spectrums that among all the concentration of all the nanofluids i.e., TiO₂, Al₂O₃, CNC, Al₂O₃/TiO₂ and Al₂O₃/CNC nanofluids, 0.9% concentration exhibits maximum absorption peak, indicating the better stability of nanofluid suspension (Phuoc and Massoudi 2009). It was noticed that the maximum absorption peak appears in range of 200-400 nm wave length for all nanofluids with all volume concentrations, however, the range is found to be 200-250 nm wave length in case of CNC nanofluids with all volume concentrations. Further, any absorption peak has not been noticed for 0.1% Al₂O₃/CNC nanofluids which may be due to the instability of nanofluid dispersion. Moreover Phuoc and Massoudi (2009), also observed and reported the similar behaviour in nanofluids which may be due to the effect of adjacent particle. After the formation of colloidal suspension, base fluid creates an upward stream which pushes the nanoparticle and prevents them from falling due to gravity acceleration. Hence, the upward stream impact is greater in high concentration than low concentration nanofluid which reduces absorbance drop in the colloidal suspension (Duangthongsuk and Wongwises 2008).

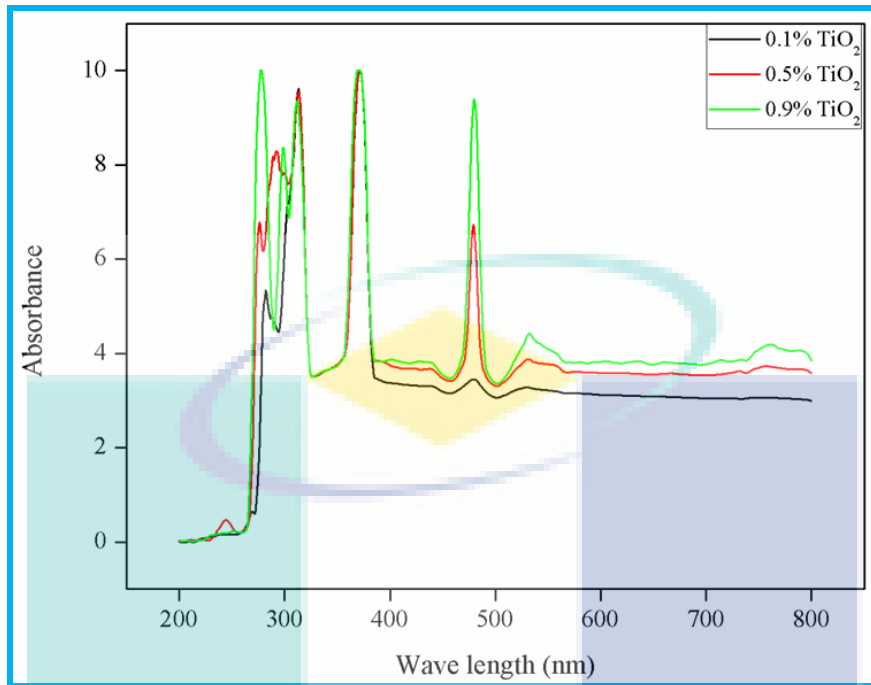


Figure 15 UV spectrum of TiO₂ nanofluid with various concentrations

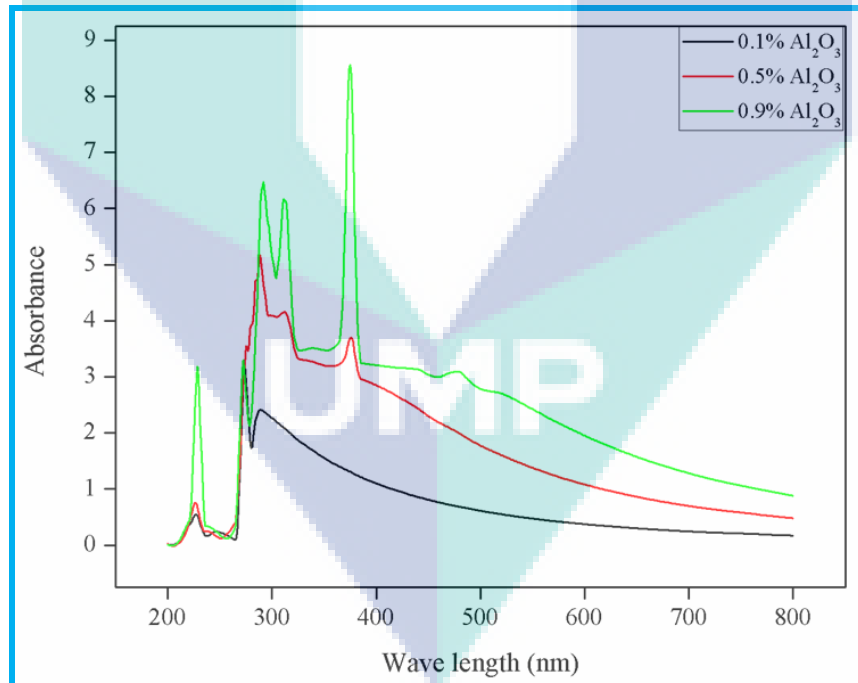


Figure 16 UV spectrum of Al₂O₃ nanofluid with various concentrations

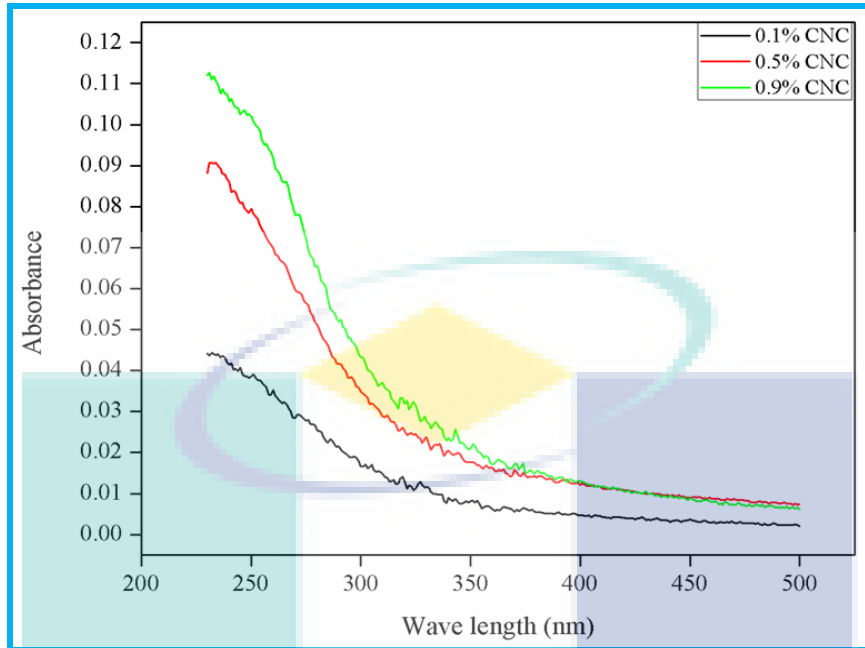


Figure 17 UV spectrum of CNC nanofluid with various concentrations

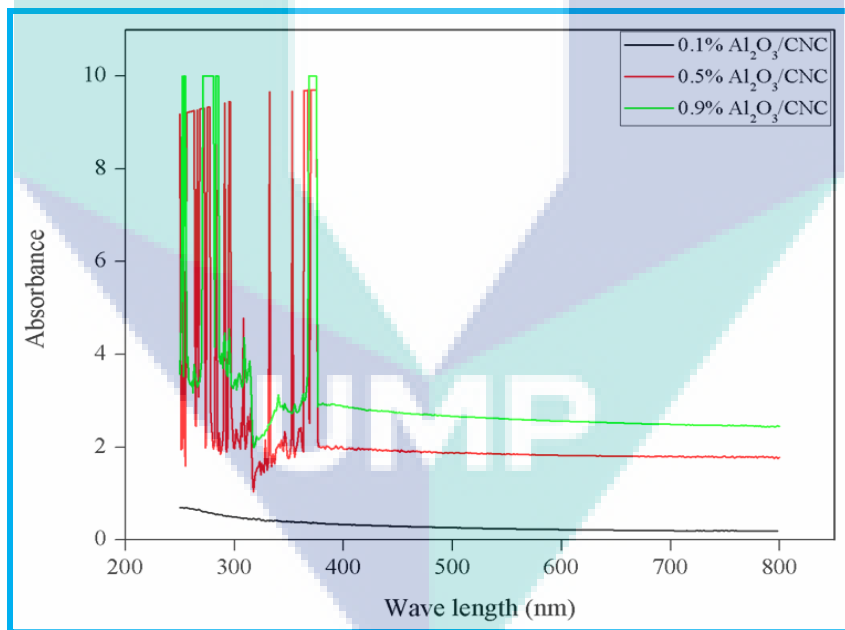


Figure 18 UV spectrum of Al₂O₃/CNC nanofluid with various concentrations

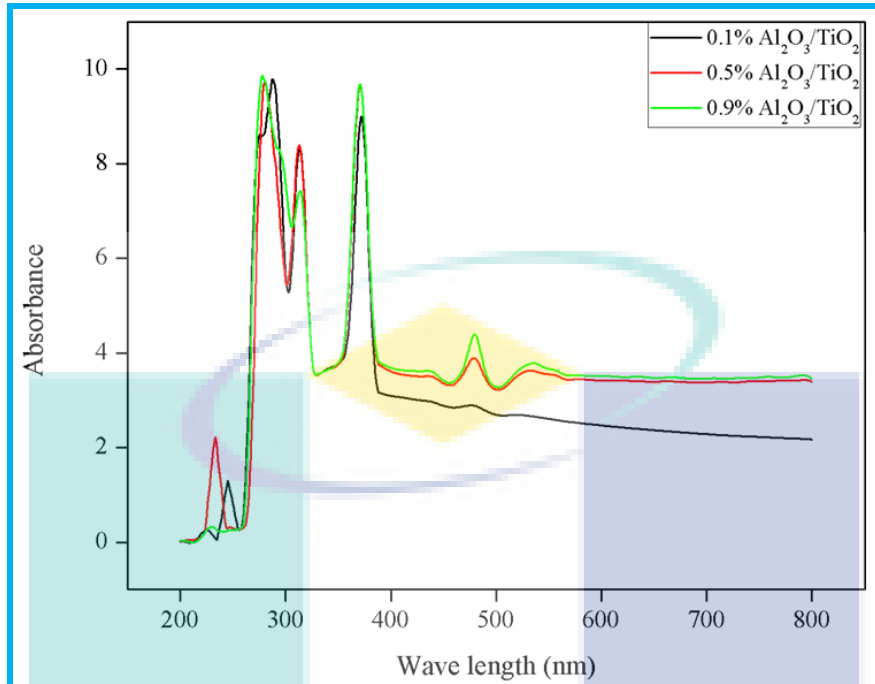


Figure 19 UV spectrum of Al₂O₃/TiO₂ nanofluid with various concentrations

The crystal structure information of all the samples was collected by recording and analysing their XRD pattern. The wide angle XRD patterns of Al₂O₃, CNC and TiO₂ nanoparticles are shown in Figure 4.11, 4.12 and 4.13, respectively. The XRD pattern shown in Figure 4.12, reveals the pure phase of CNC (C₆H₁₀O₅)_n Cellulose-1 β) nanoparticles where most intense peaks at 2θ angles of 16.6° and 22.9° correspond to the (1, 1, 0) and (2, 0, 0) crystal planes, respectively and other peaks are match well with standard XRD pattern (ICDD no. 00-056-1718) and literatures (Kumar, Negi et al. 2014).

Beside these, the XRD pattern of TiO₂ is displayed in Figure 4.13. This XRD result exhibits all the characteristics peaks i.e., at 2θ angles of 25.28° , 37.93° , 48.37° , 53.88° , and 62.72° corresponds to the (101), (103), (200), (105) and (213) respectively, are in good agreement with the standard XRD pattern (ICDD no. 00-001-0562) and the literature (Al-Taweel and Saud 2016).

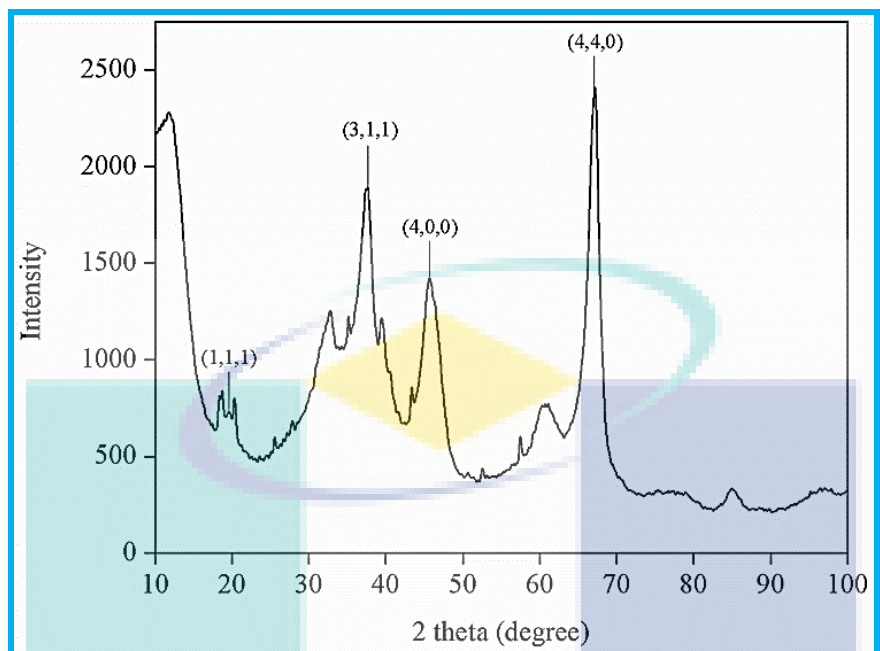


Figure 20 XRD pattern of Al₂O₃ nanoparticles

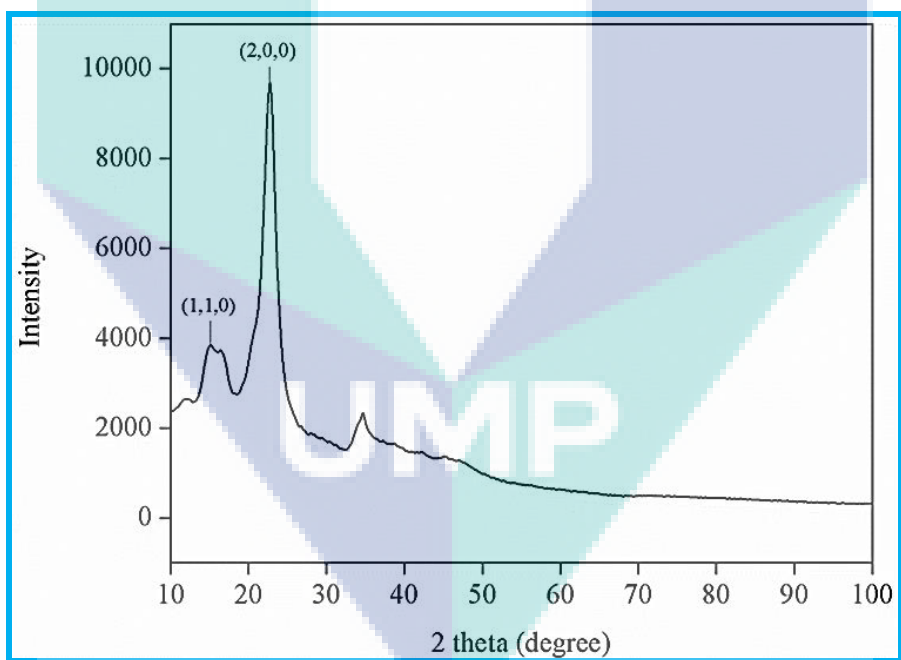


Figure 21 XRD pattern of CNC nanoparticles

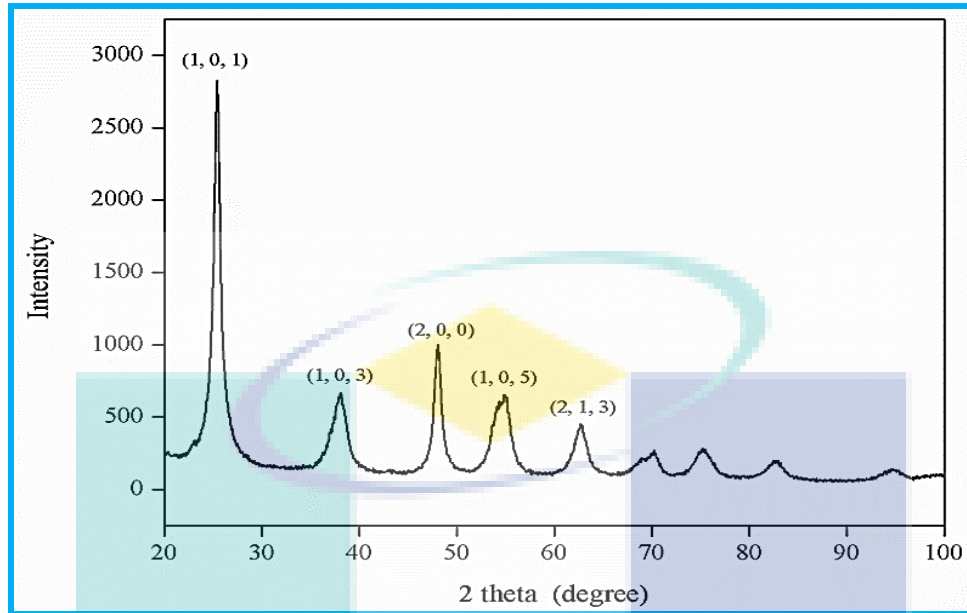


Figure 22 XRD pattern of TiO₂ nanoparticles

The FTIR spectra were recorded to investigate the chemical composition of mono and hybrid nanofluids and results are shown in Figure 4.14 and 4.15, respectively. It can be noticed from both the figures that the FTIR spectra for all the mono and hybrid nanofluids are almost identical. All the spectra of nanofluids contain a broadband in the frequency range of 3200 to 3650 cm⁻¹ and one sharp band at 1640 cm⁻¹ can be attributed to the stretching and bending mode of O-H group of EG and water, respectively. The band at around 2950 cm⁻¹ wave number in all spectra can be corresponds to stretching of C-H groups of EG (Al-Abadleh and Grassian 2003, Al-Taweel and Saud 2016, Tabesh, Davar et al. 2018). The band found at 1412 cm⁻¹ may be correspond to -CH₂ stretching of EG. On the other hand, band at 2115 cm⁻¹ can be noticed in the spectra of CNC and Al₂O₃/CNC nanofluids, can be ascribed to C≡C bonds. From both the figure, it can be observed that no band was noticed for the metal oxide (Al₂O₃ and TiO₂) in all the spectra, besides it all the bands are corresponds to the only EG with water and CNC chemical composition. Therefore, it can be concluded that no chemical reaction takes place between the base fluids and the metal oxide during the preparation.

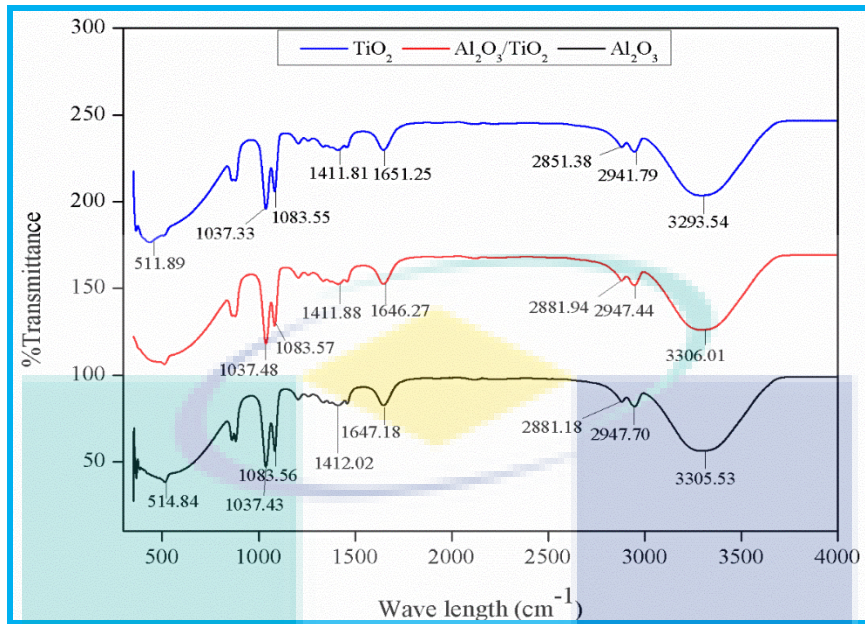


Figure 23 FTIR spectra of TiO₂, Al₂O₃ (mono) and Al₂O₃/TiO₂ (hybrid) nanofluids

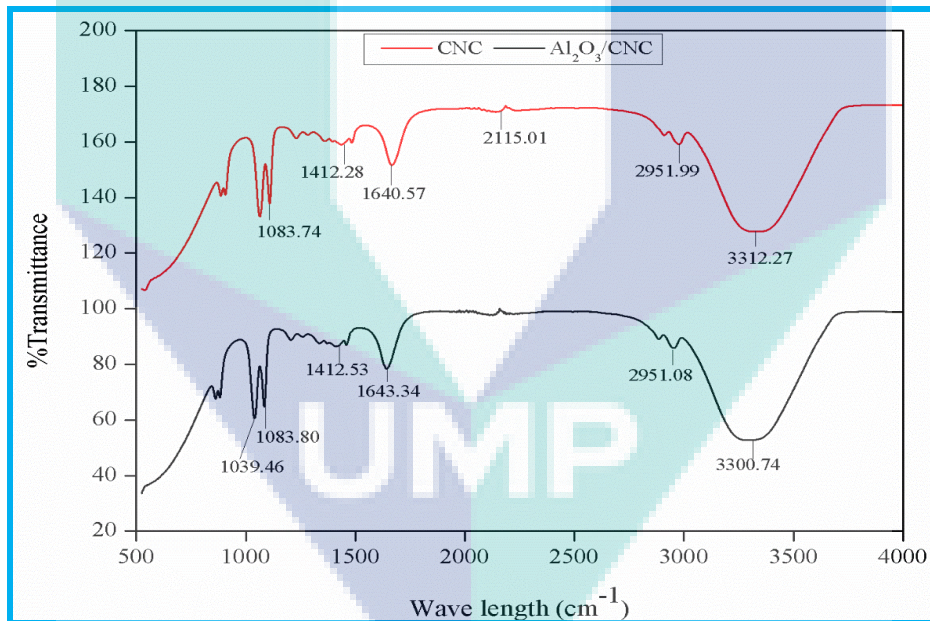


Figure 24 FTIR spectra of CNC mono and Al₂O₃/CNC hybrid nanofluid

FESEM was used to investigate the surface morphological properties of all the samples and the results are shown in Figure 4.16-4.18. Figure 4.16a and 4.16b represents the FESEM image and corresponding EDX pattern of Al₂O₃ nanoparticles, respectively. The FESEM image depicts that particles are almost spherical in shaped. These nanoparticles interconnected to each other and form large particles (microparticles) having irregular shape. The small and bigger particles have the diameter in the range of 50 to 90 nm and 1 to 5 μm, respectively. Further

elemental analysis of these particles confirms that presence of Al and O in the nanoparticles (Figure 4.16b).

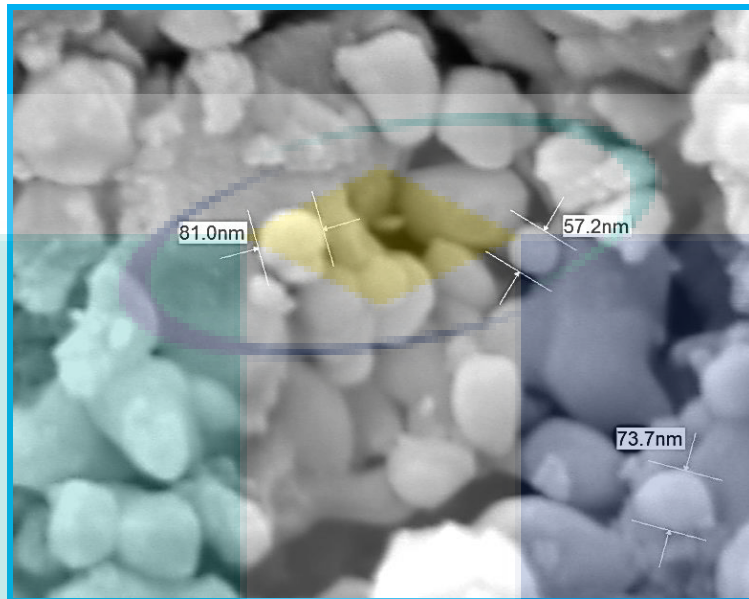


Figure 25 FESEM micrograph of Al₂O₃ nanoparticles (Magnification X100,000)

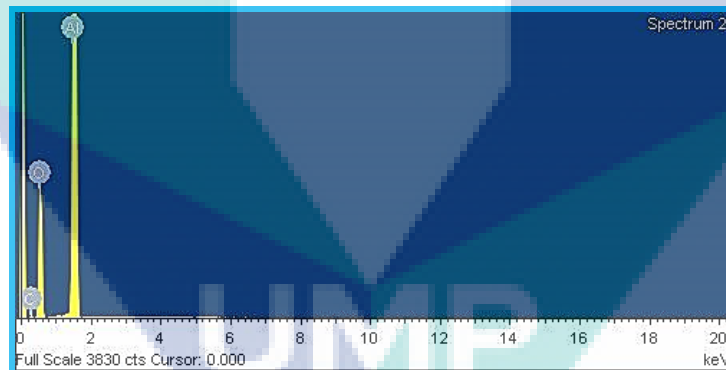


Figure 26 EDX spectrum of Al₂O₃ nanoparticles

On the other hand, CNC was in the gel form which make it difficult to analyze the topographical properties using FESEM. Therefore, two samples (i.e., film and powder) of CNC were prepared by drying for FESEM analysis and the obtained results are shown in Figure 4.17a. It can be observed from the both figures that no individual nanoparticles can be seen in both the samples. Though, particles are interconnected to each other form a porous morphology which look like net. However, EDX analysis (Figure 4.17b) confirms the presence of C and O atoms in CNC nanoparticles.

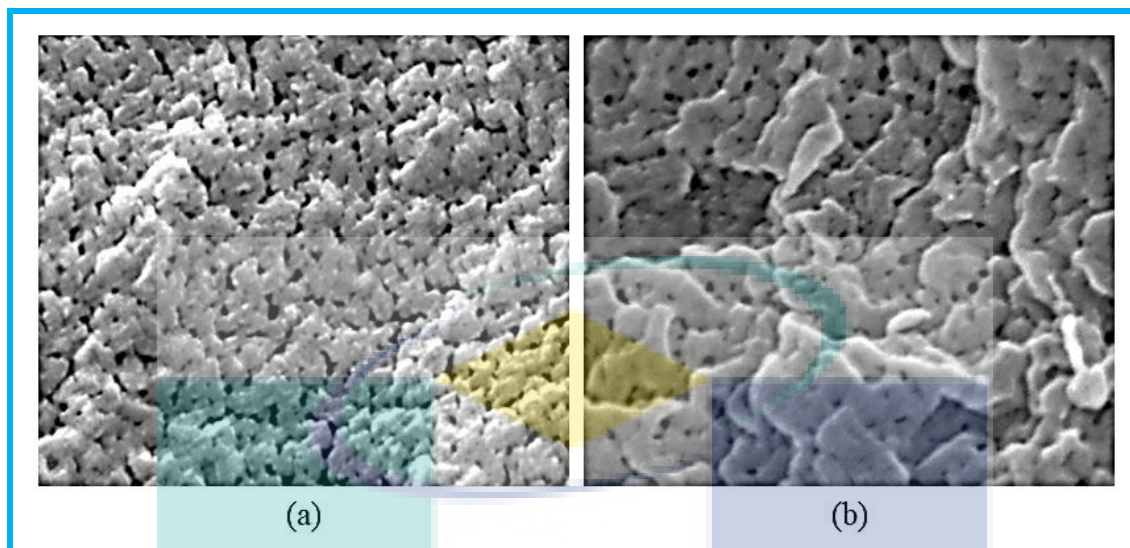


Figure 27 FESEM micrograph of CNC nanoparticles (a) Film (magnification X100,000) and (b) powder (magnification X100,000)

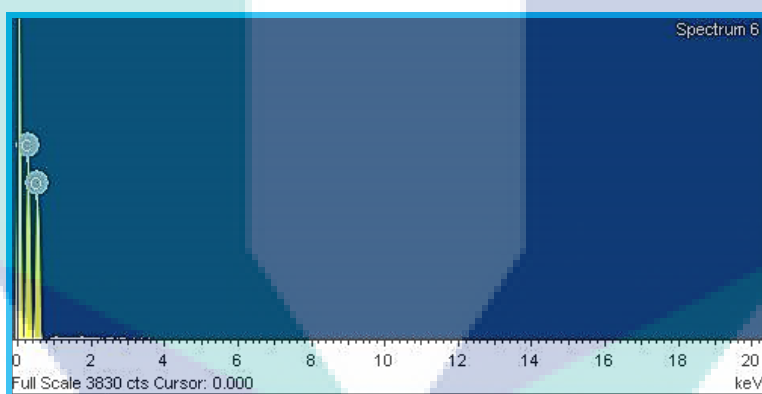


Figure 28 EDX spectrum of CNC nanoparticles

From FESEM image of TiO₂ nanoparticles (shown in Figure 4.18a) it can be seen that the shape of individual particles is spherical with the diameter below 50 nm. These nanoparticles combined to form bigger particles which look like loosely bound or not properly agglomerated. Further, EDX analysis (Figure 4.18b) indicates the presence of Ti and O atoms in the sample.

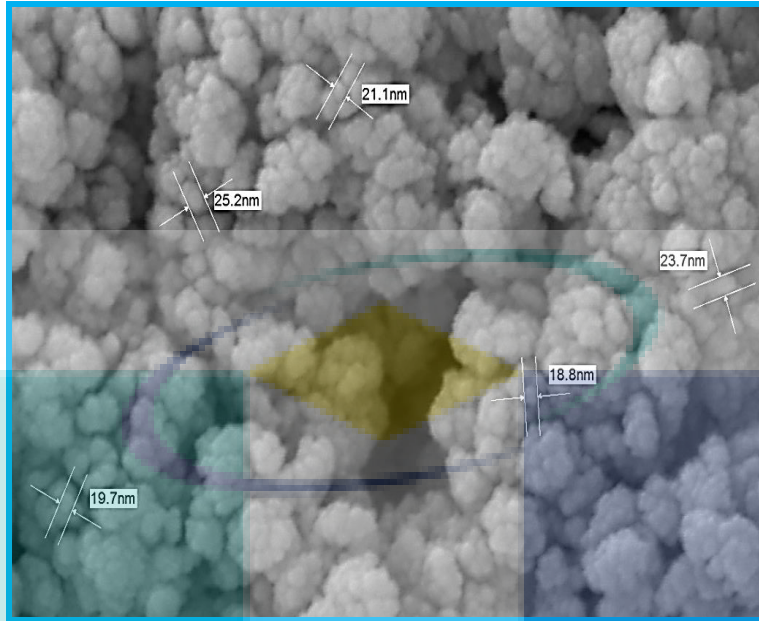


Figure 29 FESEM micrograph of TiO₂ nanoparticles (Magnification X100,000)

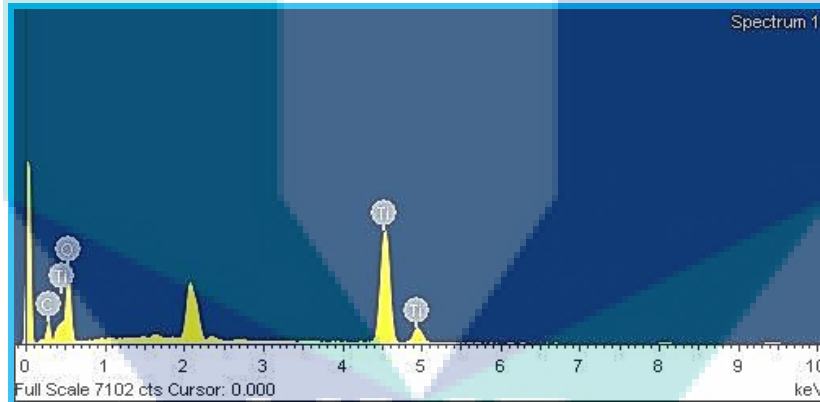


Figure 30 EDX spectrum of TiO₂ nanoparticles

It was observed from the literature that the thermal conductivity of nanofluids significantly increased on increasing the volume concentration of suspended nanoparticles in the base fluid. For instance, the thermal conductivity enhancement was observed by Fani, Kalteh et al. (2015) with increasing volume concentration of nanoparticles. They reported that the collision between the particles intensified causing an increment in the Brownian diffusivity assisting which results in thermal conductivity enhancement. The thermal conductivity of TiO₂, Al₂O₃, CNC, Al₂O₃/TiO₂, and Al₂O₃/CNC nanofluids with different volume concentration of 0.1%, 0.5%, and 0.9% were measured and the results are shown in Figure 4.19. It can be observed from the figure that the thermal conductivity of both mono and hybrid nanofluids increases on increasing volume

concentration. Further, Al₂O₃/CNC hybrid nanofluid exhibits superior thermal conductivity than other hybrid as well as mono nanofluids. It was also found that mono nanofluids (Al₂O₃) shows higher thermal conductivity improvement than CNC and TiO₂ nanofluids, due to the better thermal properties of Al₂O₃. However, increasing thermal conductivity of all nanofluids (mono and hybrid) follow the augmentation of adding of nanoparticles into the base fluid. Therefore, 0.9% volume concentration of Al₂O₃/CNC and Al₂O₃/TiO₂ show higher thermal conductivity than 0.5% and 0.1% volume concentration.

In the present study, hybrid nanofluids exhibit better thermal conductivity than mono nanofluids which may be due to the high kinetic energy generated by the high collisions of particles. Similar phenomenon have also been observed by Esfe, Esfandeh et al. (2017) for ZnO/MWCNTs/water-EG nanofluids where 28.1% higher thermal conductivity was obtained for hybrid nanofluid with 0.1% volume concentration than single phase nanofluids at 50 oC. Huang, Wu et al. (2016) have also investigated the thermal conductivity enhancement Al₂O₃ and MWCNTs dispersed into water base hybrid nanofluid in a chevron plate heat exchanger and observed a better increment in thermal conductivity than Al₂O₃ nanofluid and water. Since the particles are capable of transferring heat directly from one to another at high temperature, therefore, high temperature increases the rate of heat transfer. At high temperature, the Brownian motion of particles increases due to high kinetic energy which then enhances the thermal conductivity (Duangthongsuk and Wongwises 2008, Fani, Kalteh et al. 2015). The maximum thermal conductivity have been achieved at 60oC in the present work. For instance, on increasing the temperature from 30oC to 60oC, thermal conductivity of Al₂O₃/CNC hybrid nanofluid increased from 0.57 to 0.59 W/m-K in 0.9% volume fraction (Figure 4.19).

Similar work have also been reported in the literature. For example, Nabil, Azmi et al. (2017) observed an enhancement in thermal conductivity of 22.8% for TiO₂-SiO₂/water and EG hybrid nanofluid in 3% volume fraction at 80oC temperature which is much better than observed by Hamid, Azmi et al. (2018) for TiO₂-SiO₂/water and EG hybrid nanofluid (22.1%) 70oC. Further, Hamid, Azmi et al. (2018) have also reported that thermal conductivity increased from 13.8 % to 16 % for SiO₂-TiO₂/water and EG hybrid nanofluid in 1% volume fraction on increasing the temperature from 70 oC to 80 oC.

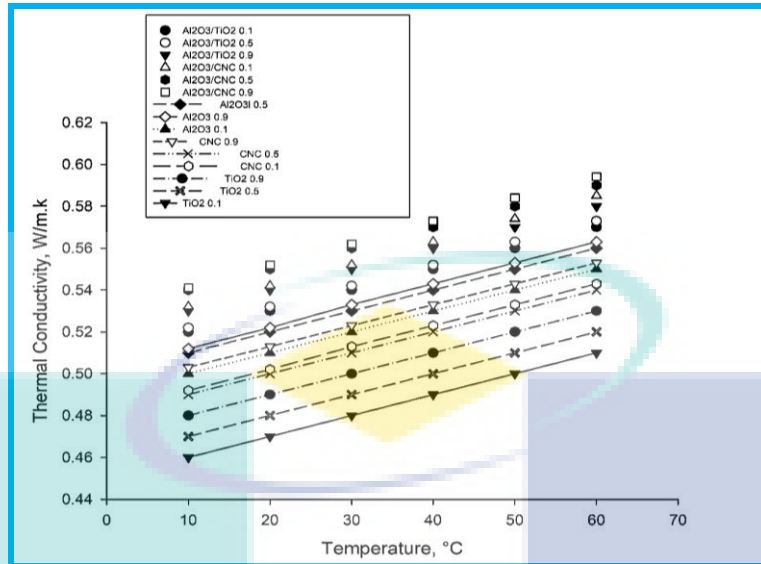


Figure 31 Thermal conductivity of all nanofluids vs. temperature plot

Almost all correlation related to thermal conductivity of hybrid nanofluid, constructed based on experiment are highly influenced by temperature and volume fraction of nanoparticles. These established corrections are applicable for narrow range of depending parameters such as temperature and concentration of hybrid nanofluid. Basically, all studies describe that increasing temperature and volume fraction would increase thermal conductivity of nanofluid due to increasing kinetic energy as well as rate of collision and clustering of nano-additive, respectively. Extended research is necessary to develop a model that included all the factors required for prediction of thermal conductivity.

Initially, the viscosity of base fluid was measured in order to verify the correct steps and to obtain accurate data. According to Vajjha, Das et al. (2010), the mixture of water and EG shows Newtonian behaviour which govern the rheological property and the nanofluids behave like Newtonian. The viscosity of all the nanofluids (mono and hybrid) was measured and the obtained results are shown in Figure 4.20. It can be observed from the figure that the viscosity of nanofluids are higher than the base fluid for both mono and hybrid nanofluids. As the concentration increased, the viscosity also increases. Hybrid nanofluids such as Al₂O₃/CNC and Al₂O₃/TiO₂ exhibit higher viscosity than the mono nanofluids (Al₂O₃, CNC and TiO₂) with all volume concentrations. However, Al₂O₃/CNC nanofluid dominates the viscosity over the viscosity of Al₂O₃/TiO₂ for all volume concentrations. On the other hand, the viscosity of Al₂O₃ nanofluids at various volume fraction is found to be higher than CNC and TiO₂ nanofluids. A similar effect of volume concentration to the viscosity has also been observed by Namburu, Kulkarni et al. (2007) and Fedele, Colla et al. (2012). However, viscosity of 0.1% volume concentration is higher than 0.9% volume fraction of Al₂O₃ nanofluid which does not support the previous literature of viscosity. Similarly, 0.1% CNC nanofluid exhibits higher viscosity than 0.5% CNC nanofluid.

It is also noticed from the figure that viscosity decreases on increasing the temperature. For instance, the viscosity of both hybrid (Al₂O₃/CNC and Al₂O₃/TiO₂) nanofluids at all volume concentrations is gradually decreases on increasing the temperature and found lowest at 70 oC temperature. Whereas the mono nanofluids (Al₂O₃, CNC, and TiO₂) with all volume concentrations except 0.1% and 0.5% TiO₂ nanofluids exhibits the lowest viscosity at 50 oC temperature which shows increasing trend at 70oC. The effect of temperature on viscosity of nanofluids was clarified by Li, Zou et al. (2015) on the basis of molecular viewpoint and reported that the intermolecular distance increases on rising the temperature which leads to the diminished pattern of the viscosity.

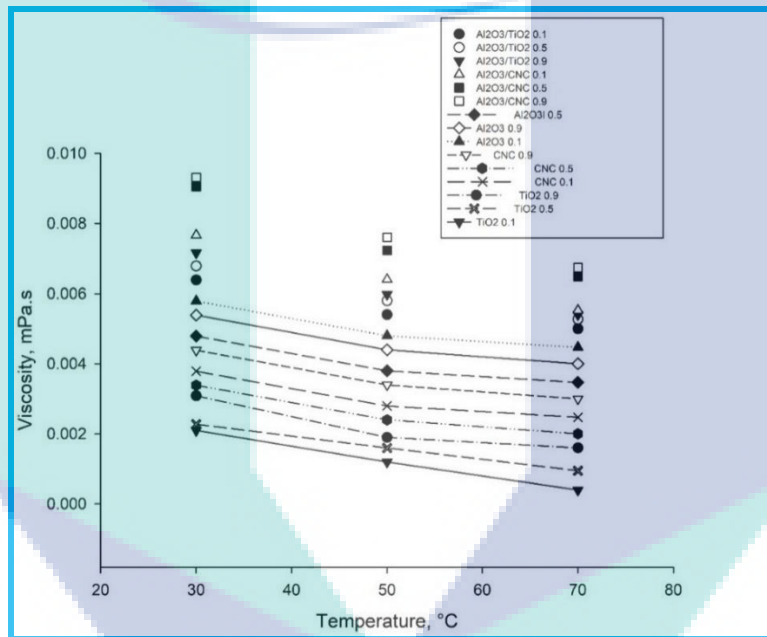


Figure 32 Viscosity with respect to temperature

Basically, the base fluid plays an important role in the density of nanofluids. Density of nanofluids is also depends on temperature (Vajjha, Das et al. 2009). The density of mono and hybrid (Al₂O₃, TiO₂, CNC, Al₂O₃/TiO₂, and Al₂O₃/CNC) nanofluids was measured by varying the temperature and volume concentration and obtained results are shown in Figure 4.21. It can be noticed from the figure that density of all nanofluids (mono and hybrid) was increase on adding nanoparticles into the base fluid which further gradually increased on loading augmentation of nanoparticles. However, only 0.5% volume fraction of Al₂O₃ nanofluid exhibited higher density than 0.9% Al₂O₃ nanofluid. Although, the maximum density of all mono and hybrid nanofluids was observed at 30 °C temperature which gradually decreases till 70 °C temperature. However, 0.1% CNC nanofluid contains slightly higher density at 70 oC than at 50 oC temperature. Both hybrid nanofluids (Al₂O₃/TiO₂, and Al₂O₃/CNC) show the uppermost density value than the

mono nanofluids (Al_2O_3 , TiO_2 , and CNC). Although, $\text{Al}_2\text{O}_3/\text{TiO}_2$ hybrid nanofluids portrayed superior density than other mono (Al_2O_3 , TiO_2 , and CNC) and hybrid ($\text{Al}_2\text{O}_3/\text{CNC}$) nanofluids.

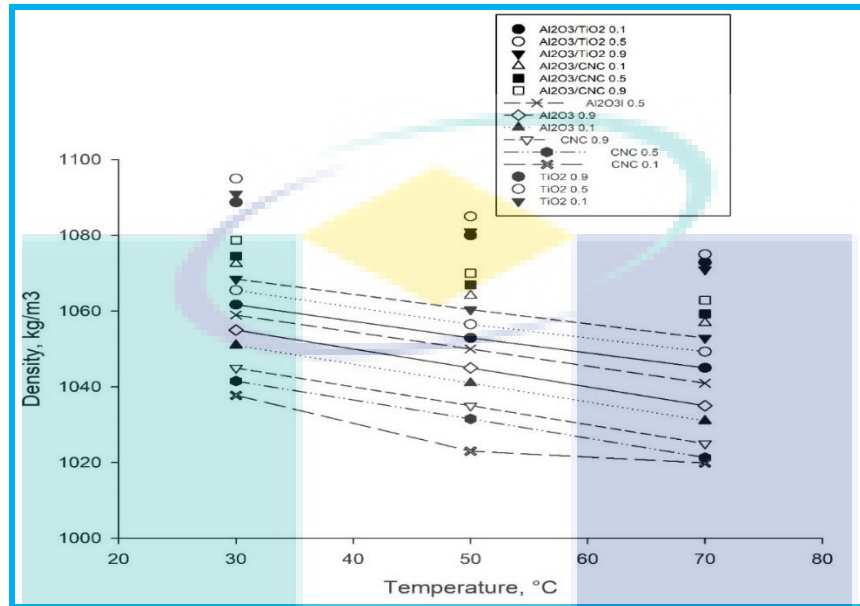


Figure 33 Density comparison as a function of temperature and volume

Specific heat capacity is another vital thermo-physical property of nanofluids to observe their heat transfer performance. A number of theoretical and experimental studies has been carried out to determine the specific heat capacity of nanofluids (mono and hybrid) at different temperature and volume concentrations. O'Hanley, Buongiorno et al. (2012) investigated the effect of various volume concentrations on the specific heat capacity of different types of nanofluids (such as water-based alumina, silica, copper-oxide) and reported that specific heat capacity decreased on increase the volume fractions of nanofluids. Furthermore, Singh, Sharma et al. (2017) observed that the specific heat of nanofluids decrease at room temperature with increasing the concentration of nanoparticles and found to be minimum at the highest temperature.

The specific heat capacity of Al_2O_3 , CNC , TiO_2 , $\text{Al}_2\text{O}_3/\text{CNC}$, and $\text{Al}_2\text{O}_3/\text{TiO}_2$ nanofluids was measure as a function of temperature and volume concentration and obtained results are shown in Figure 4.22. It has been observed from the results that all the nanofluids (mono and hybrid) exhibit low and high specific heat at 30°C and 90°C temperature, respectively. Further, $\text{Al}_2\text{O}_3/\text{CNC}$ hybrid nanofluid shows lowest specific heat capacity than other hybrid nanofluid. On the other hand, CNC nanofluids (all volume concentrations) displayed the highest specific heat capacity than other mono nanofluids. In case of CNC nanofluids, 0.5% CNC nanofluid exhibits highest specific heat value than rest of concentration of CNC . On the contrary, 0.1% Al_2O_3 nanofluid depicts the uppermost specific heat capacity than other concentration of Al_2O_3

nanofluids. It was observed from the above discussion that these results are not consistent with typical research proposal. However, the better specific heat capacity value exhibited by CNC nanoparticles is surprising result. Furthermore, nanofluid with CNC nanoparticles shows the highest specific heat capacity as compared to nanofluids with hybrid nanoparticles at 30 °C temperature. Over all, it was noticed from the Figure 4.22 that specific heat capacity directly and inversely proportional to the temperature and volume concentration. Similar results have also been observed by Zhou and Ni (2008). Basically, volume concentration has more impact than temperature on specific heat capacity measurement (Sekhar and Sharma 2015). Moreover, specific heat capacity is more effective in heat transfer application than the thermal conductivity (Shin and Banerjee 2014). Therefore, nanofluid with enhanced specific heat capacity is required for an efficient thermal exchange application.

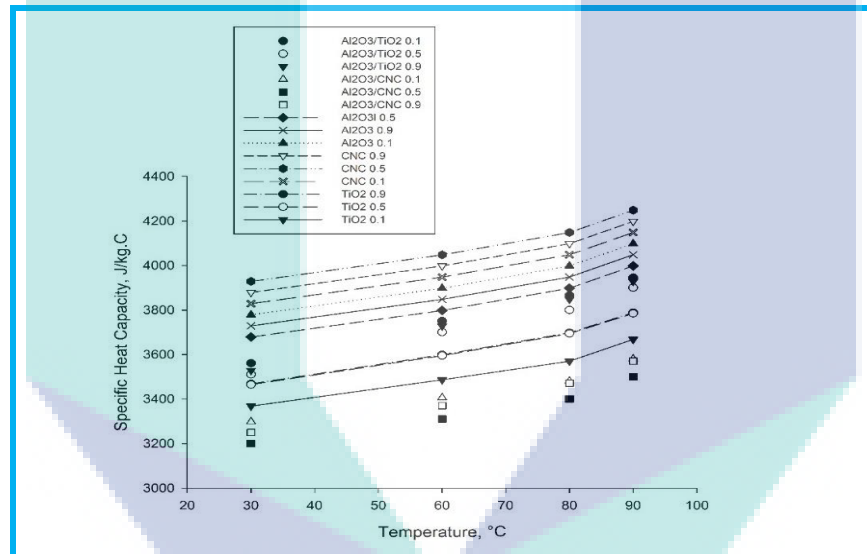


Figure 34 Comparison of specific heat capacity of mono and hybrid nanofluids with various volume concentrations

MD simulations in this study were performed using large-scale atomic/molecular massively parallel simulator, LAMMPS. The simulation carried out on solid cylindrical shaped graphene, which were subjected to uniaxial tensile strain in the [1 0 0] direction. The nanowires with a cylindrical configuration, as shown in Figure 35, were selected because of stability and natural cross-sectional configuration. The initial atomic configuration is positioned at the fcc lattice sites. The X, Y, Z coordinates axes represent the lattice direction of [1 0 0], [0 1 0], [0 0 1] respectively. A periodic boundary condition was applied in the length direction, X-direction, while the Y and Z directions were left as free surfaces. The temperature in each simulation is kept constant at 300 K. Eight graphene models with the same diameter of 7.04 nm and different lengths of 17.60 nm, 21.12 nm, 24.64 nm, 28.16 nm, 31.68 nm, 35.20 nm, 52.80 nm and 70.40 nm respectively.

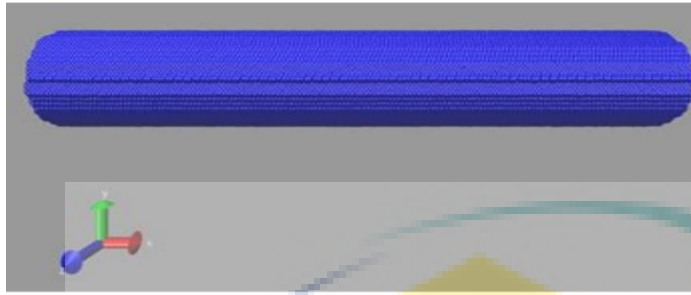


Figure 35 nanowires with a cylindrical configuration

The visual molecular dynamics (VMD) software is used to visualize the activities carried out in molecular dynamics simulations. Figure 36 shows the deformation of a 35.2 nm long graphene during the stretching process at a temperature of 300 K and strain rate of 0.0001 ps^{-1} . After being fully relaxed, some of the graphene atoms on the nanowire surface are rearranged, resulting in some local lattice defects. During the application of the load, it is observed that the surface of the nanowire is cracked abruptly and some lattices slide on the cracking area resulting in the necking shape until it deforms into the final rupture.

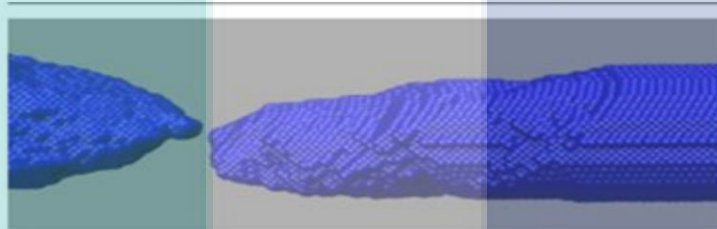


Figure 36 shows the deformation of a 35.2 nm

References

ACHIEVEMENT

i) Name of articles/ manuscripts/ books published

1. Impact of stabilization environment and heating rates on P84 co-olyimide/nanocrystalline cellulose carbon membrane for hydrogen enrichment

2. P84 Co-Polyimide-based Tubular Carbon Membrane: Effect of Pyrolysis Temperature

3. Tubular Carbon Membrane Prepared from PI/NCC: Effects of Pyrolysis Atmosphere
Effect of heating rates on the microstructure and gas permeation properties of carbon membranes

4. Thermal Performance of Hybrid-Inspired Coolant for Radiator Application

5. PI/NCC-Based Tubular Carbon Membrane: Influence of Aging Times Towards Oxygen Separation Performance

ii) Title of Paper presentations (international/ local)

iii) Human Capital Development

1. Norhanis Sofiah - PhD
2. Sakinah Hisham - PhD

iv) Awards/ Others
Gold medal - Citrex exhibition

v) Others
Patent filing - PI2019002239

REFERENCES

Abdolbaghi, S., A. Namjoo, Y. Saadat and S. Hosseinzadeh (2016). "Fabrication of cage-like particles via unstable seeded dispersion polymerization: A new concept in the polymerization-induced self-assembly." *Journal of Macromolecular Science, Part A* 53(2): 116-124.

Afrand, M., D. Toghraie and B. Ruhani (2016). "Effects of temperature and nanoparticles concentration on rheological behavior of Fe₃O₄-Ag/EG hybrid nanofluid: an experimental study." *Experimental Thermal and Fluid Science* 77: 38-44.

Al-Abadleh, H. A. and V. Grassian (2003). "FT-IR study of water adsorption on aluminum oxide surfaces." *Langmuir* 19(2): 341-347.

Al-Taweel, S. S. and H. R. Saud (2016). "New route for synthesis of pure anatase TiO₂ nanoparticles via ultrasound assisted sol-gel method." *Journal of Chemical and Pharmaceutical Research* 8(2): 620-626.

Alauddin, M., M. El Baradie and M. Hashmi (1995). "Computer-aided analysis of a surface-roughness model for end milling." *Journal of Materials Processing Technology* 55(2): 123-127.

Allahyar, H., F. Hormozi and B. ZareNezhad (2016). "Experimental investigation on the thermal performance of a coiled heat exchanger using a new hybrid nanofluid." *Experimental Thermal and Fluid Science* 76: 324-329.

Amrutkar, P. S. and S. R. Patil (2013). "Automotive radiator performance-Review." *International Journal of Engineering and Advanced Technology* 2(3): 563-565.

Angayarkanni, S. and J. Philip (2015). "Review on thermal properties of nanofluids: Recent developments." *Advances in colloid and interface science* 225: 146-176.

ASHRAE, A. (2005). "Handbook of fundamentals." American Society of Heating Refrigerating and Air Conditioning Engineers, Atlanta, GA.

Azmi, W., K. A. Hamid, R. Mamat, K. Sharma and M. Mohamad (2016). "Effects of working temperature on thermo-physical properties and forced convection heat transfer of TiO₂ nanofluids in water–Ethylene glycol mixture." *Applied Thermal Engineering* 106: 1190-1199.

Azmi, W., K. A. Hamid, N. Usri, R. Mamat and M. Mohamad (2016). "Heat transfer and friction factor of water and ethylene glycol mixture based TiO₂ and Al₂O₃ nanofluids under turbulent flow." *International Communications in Heat and Mass Transfer* 76: 24-32.

Baradie, M. E. (1993). "Surface roughness model for turning grey cast iron (154 BHN)." *Proceedings of the Institution of Mechanical Engineers, Part B: Journal of Engineering Manufacture* 207(1): 43-54.

Batchelor, G. (1977). "The effect of Brownian motion on the bulk stress in a suspension of spherical particles." *Journal of fluid mechanics* 83(1): 97-117.

Bhanvase, B., M. Sarode, L. Putterwar, K. Abdullah, M. Deosarkar and S. Sonawane (2014). "Intensification of convective heat transfer in water/ethylene glycol based nanofluids containing TiO₂ nanoparticles." *Chemical Engineering and Processing: Process Intensification* 82: 123-131.

Bhatt, R., H. Patel and O. Vashi (2014). "Nano fluids: a new generation coolants." *Int J Res Mech Eng Technol* 4: 16-22.

Boothroyd, G. (1988). *Fundamentals of metal machining and machine tools*, Crc Press.

Box, G. E. and N. R. Draper (1987). *Empirical model-building and response surfaces*, John Wiley & Sons.

Brinkman, H. (1952). "The viscosity of concentrated suspensions and solutions." *The Journal of Chemical Physics* 20(4): 571-571.

Choi, S. U. and J. A. Eastman (1995). *Enhancing thermal conductivity of fluids with nanoparticles*, Argonne National Lab., IL (United States).

Choudhury, I. and M. El-Baradie (1999). "Machinability assessment of inconel 718 by factorial design of experiment coupled with response surface methodology." *Journal of Materials Processing Technology* 95(1-3): 30-39.

Das, S. K., N. Putra, P. Thiesen and W. Roetzel (2003). "Temperature dependence of thermal conductivity enhancement for nanofluids." *Journal of heat transfer* 125(4): 567-574.

Dhaiban, H. T. (2016). "Numerical Study of Heat Transfer Enhancement in Heat Exchanger Using AL2O3 Nanofluids." *Journal of Engineering* 22(4): 98-115.

Diaz, G., M. Sen, K. Yang and R. L. McClain (1999). "Simulation of heat exchanger performance by artificial neural networks." *Hvac&R Research* 5(3): 195-208.

Duangthongsuk, W. and S. Wongwises (2008). "Effect of thermophysical properties models on the predicting of the convective heat transfer coefficient for low concentration nanofluid." *International Communications in Heat and Mass Transfer* 35(10): 1320-1326.

Efevbokhan, V. E. and O. N. Ohiozua (2013). "Comparison of the cooling effects of a locally formulated car radiator coolant with water and a commercial coolant." *The International Journal of Engineering and Science* 2(1): 254-262.

El-Khabeery, M. and M. Fattouh (1989). "Residual stress distribution caused by milling." *International Journal of Machine Tools and Manufacture* 29(3): 391-401.

Esfe, M. H., S. Esfandeh and S. Niazi (2019). "An experimental investigation, sensitivity analysis and RSM analysis of MWCNT (10)-ZnO (90)/10W40 nanofluid viscosity." *Journal of Molecular Liquids* 288: 111020.

Esfe, M. H., S. Esfandeh, S. Saedodin and H. Rostamian (2017). "Experimental evaluation, sensitivity analyzation and ANN modeling of thermal conductivity of ZnO-MWCNT/EG-water hybrid nanofluid for engineering applications." *Applied Thermal Engineering* 125: 673-685.

Fani, B., M. Kalteh and A. Abbassi (2015). "Investigating the effect of Brownian motion and viscous dissipation on the nanofluid heat transfer in a trapezoidal microchannel heat sink." *Advanced Powder Technology* 26(1): 83-90.

Fedele, L., L. Colla and S. Bobbo (2012). "Viscosity and thermal conductivity measurements of water-based nanofluids containing titanium oxide nanoparticles." *international journal of refrigeration* 35(5): 1359-1366.

Fortunati, E., I. Armentano, Q. Zhou, D. Puglia, A. Terenzi, L. A. Berglund and J. Kenny (2012). "Microstructure and nonisothermal cold crystallization of PLA composites based on silver nanoparticles and nanocrystalline cellulose." *Polymer degradation and stability* 97(10): 2027-2036.

Fortunati, E., M. Peltzer, I. Armentano, L. Torre, A. Jiménez and J. Kenny (2012). "Effects of modified cellulose nanocrystals on the barrier and migration properties of PLA nanobiocomposites." *Carbohydrate polymers* 90(2): 948-956.

Fuh, K.-H. and C.-F. Wu (1995). "A proposed statistical model for surface quality prediction in end-milling of Al alloy." *International Journal of Machine Tools and Manufacture* 8(35): 1187-1200.

Giovanola, J. H. (1988). "Adiabatic shear banding under pure shear loading part i: direct observation of strain localization and energy dissipation measurements." *Mechanics of Materials* 7(1): 59-71.

Hadadian, M., S. Samiee, H. Ahmadzadeh and E. K. Goharshadi (2013). "Nanofluids for heat transfer enhancement—a review." *Physical chemistry research* 1(1): 1-33.

Hamid, K. A., W. Azmi, M. Nabil and R. Mamat (2018). "Experimental investigation of nanoparticle mixture ratios on TiO₂–SiO₂ nanofluids heat transfer performance under turbulent flow." *International Journal of Heat and Mass Transfer* 118: 617-627.

Hasegawa, M., A. Seireg and R. Lindberg (1976). "Surface roughness model for turning." *Tribology international* 9(6): 285-289.

Hatami, M., M. Jafaryar, J. Zhou and D. Jing (2017). "Investigation of engines radiator heat recovery using different shapes of nanoparticles in H₂O/(CH₂OH)₂ based nanofluids." *International Journal of Hydrogen Energy* 42(16): 10891-10900.

Heris, S. Z., M. N. Esfahany and S. G. Etemad (2007). "Experimental investigation of convective heat transfer of Al₂O₃/water nanofluid in circular tube." *International Journal of Heat and Fluid Flow* 28(2): 203-210.

Hill, W. J. and W. G. Hunter (1966). "A review of response surface methodology: a literature survey." *Technometrics* 8(4): 571-590.

Huang, D., Z. Wu and B. Sunden (2016). "Effects of hybrid nanofluid mixture in plate heat exchangers." *Experimental Thermal and Fluid Science* 72: 190-196.

Jack, T. K. and M. M. Ojapah (2013). "Water-Cooled Petrol engines: A Review of Considerations in Cooling Systems Calculations With variable Coolant Density and Specific Heat." *International Journal of Advances in Engineering & Technology* 6(2): 659.

Kadrigama, K., M. Noor and M. Rahman (2008). "Optimization of surface roughness in end milling on mould aluminium alloys (AA6061-T6) using response surface method and radian basis function network." *Jourdan Journal of Mechanical and Industrial Engineering* 2(4).

Kasaeipoor, A., E. H. Malekshah and L. Kolsi (2017). "Free convection heat transfer and entropy generation analysis of MWCNT-MgO (15%– 85%)/Water nanofluid using Lattice Boltzmann method in cavity with refrigerant solid body-Experimental thermo-physical properties." *Powder technology* 322: 9-23.

Khuri, A. I. and J. A. Cornell (1996). *Response surfaces: designs and analyses*, CRC press.

Konermann, L. and D. Douglas (1997). "Acid-induced unfolding of cytochrome c at different methanol concentrations: electrospray ionization mass spectrometry specifically monitors changes in the tertiary structure." *Biochemistry* 36(40): 12296-12302.

Kumar, A., Y. S. Negi, V. Choudhary and N. K. Bhardwaj (2014). "Characterization of cellulose nanocrystals produced by acid-hydrolysis from sugarcane bagasse as agro-waste." *Journal of Materials Physics and Chemistry* 2(1): 1-8.

Kumar, M. S., V. Vasu and A. V. Gopal (2016). "Thermal conductivity and rheological studies for Cu–Zn hybrid nanofluids with various basefluids." *Journal of the Taiwan Institute of Chemical Engineers* 66: 321-327.

Lee, J. and I. Mudawar (2007). "Assessment of the effectiveness of nanofluids for single-phase and two-phase heat transfer in micro-channels." *International Journal of Heat and Mass Transfer* 50(3-4): 452-463.

Leong, K., R. Saidur, S. Kazi and A. Mamun (2010). "Performance investigation of an automotive car radiator operated with nanofluid-based coolants (nanofluid as a coolant in a radiator)." *Applied Thermal Engineering* 30(17-18): 2685-2692.

Li, X., C. Zou, T. Wang and X. Lei (2015). "Rheological behavior of ethylene glycol-based SiC nanofluids." *International journal of heat and mass transfer* 84: 925-930.

Lundgren, T. S. (1972). "Slow flow through stationary random beds and suspensions of spheres." *Journal of Fluid Mechanics* 51(2): 273-299.

Matsumoto, Y., M. Barash and C. Liu (1986). "Effect of hardness on the surface integrity of AISI 4340 steel." *Journal of Engineering for Industry* 108(3): 169-175.

Mead, R. and D. Pike (1975). "A biometrics invited paper. A review of response surface methodology from a biometric viewpoint." *Biometrics* 31(4): 803-851.

Mintsa, H. A., G. Roy, C. T. Nguyen and D. Doucet (2009). "New temperature dependent thermal conductivity data for water-based nanofluids." *International Journal of Thermal Sciences* 48(2): 363-371.

The logo of UMP (Université de Montpellier) is a large, stylized shield shape. It is divided into four quadrants by a white cross. The top-left quadrant is light blue, the top-right is light purple, the bottom-left is light purple, and the bottom-right is light blue. In the center of the shield, the letters 'UMP' are written in a bold, white, sans-serif font.

UMP